Isolating perturbative QCD splittings in heavy-ion collisions

Leticia Cunqueiro,[1] Daniel Pablos,[2,3,4] Alba Soto-Ontoso,[5] Martin Spousta,[6] Adam Takacs,[7,8] and Marta Verweij[9,10]

[1]*Sapienza Università di Roma & INFN, Piazzale Aldo Moro 5, Roma 00185, Italy*
[2]*INFN, Sezione di Torino, via Pietro Giuria 1, I-10125 Torino, Italy*
[3]*Departamento de Física, Universidad de Oviedo, Avda. Federico García Lorca 18, 33007 Oviedo, Spain*
[4]*Instituto Universitario de Ciencias y Tecnologías Espaciales de Asturias (ICTEA), Calle de la Independencia 13, 33004 Oviedo, Spain*
[5]*CERN, Theoretical Physics Department, CH-1211 Geneva 23, Switzerland*
[6]*Institute of Particle and Nuclear Physics, Faculty of Mathematics and Physics, Charles University, V Holešovičkách 2, 180 00 Prague 8, Czech Republic*
[7]*Department of Physics and Technology, University of Bergen, Allegaten 55, 5007 Bergen, Norway*
[8]*Institute for Theoretical Physics, Heidelberg University, Philosophenweg 16, 69120 Heidelberg, Germany*
[9]*Institute for Gravitational and Subatomic Physics (GRASP), Utrecht University, Utrecht, Netherlands*
[10]*Nikhef, National institute for subatomic physics, Amsterdam, Netherlands*

(Received 20 December 2023; accepted 29 May 2024; published 10 July 2024)

We define a new strategy to scan jet substructure in heavy-ion collisions. The scope is multifold: (i) test the dominance of vacuum jet dynamics at early times, (ii) capture the transition from coherent to incoherent jet energy loss, and (iii) study elastic scatterings in the medium, which are either hard and perturbative or soft and responsible for jet thermalization. To achieve that, we analyze the angular distribution of the hardest splitting, $\theta_{\rm hard}$, above a transverse momentum scale, $k_t^{\rm min}$, in high-p_t jets. Sufficiently high values of $k_t^{\rm min}$ target the regime in which the observable is uniquely determined by vacuumlike splittings and energy loss, leaving the jet substructure unmodified compared to proton-proton collisions. Decreasing $k_t^{\rm min}$ enhances the sensitivity to the relation between energy loss and the intrajet structure and, in particular, to observe signatures of color decoherence at small angles. At wider angles it also becomes sensitive to hard elastic scatterings with the medium and, therefore, the perturbative regime of medium response. Choosing $k_t^{\rm min} \approx 0$ leads to order one effects of nonperturbative origin such as hadronization and, potentially, soft scatterings responsible for jet thermalization. We perform a comprehensive analysis of this observable with three state-of-the-art jet-quenching Monte Carlo event generators. Our study paves the way for defining jet observables in heavy-ion collisions dominated by perturbative QCD and thus calculable from first principles.

DOI: 10.1103/PhysRevD.110.014015

I. INTRODUCTION

Collisions of heavy ions at ultrarelativistic energies produce a myriad of particles [$\mathcal{O}(10^3)$]. The presence of a quark-gluon plasma (QGP) phase during the system evolution leaves an imprint on the characteristic pattern of final state multiparticle correlations. The ultimate goal of the heavy-ion program is to characterize the QGP in terms of its transport properties and microscopic structure. One of the main challenges is to design and measure observables that are both QGP standard candles and amenable to theoretical computations. A successful approach to this problem is the use of jet observables to measure their modification compared to jets in proton-proton collisions. Experimental overviews on jet modification are provided in Refs. [1–5], while for theory see Refs. [6–8]. While early measurements used jets as monolithic objects, most recent measurements focus on the internal structure of jets (see Refs. [2–4] for more details). The main model-agnostic conclusion that can be drawn from these measurements is that in-medium jets lose around 10% of their energy, i.e., are quenched, by means of copious out-of-cone radiation induced by the QGP and that this energy degradation is sensitive to the jet substructure.

The theoretical description of some of the key processes in jet formation in heavy-ion collisions is in the realm of perturbative QCD (pQCD) and is thus calculable. Effects that pertain to this category are, e.g., nuclear-modified

parton distribution functions [9–11], the initial hard-scattering (prior to QGP formation), and early vacuumlike QCD radiation [12,13]. Medium-induced emissions, triggered by the interaction between the jet particles and the QGP color fields [14–17], in most cases, are assumed to be perturbative. Their description requires phenomenological input, namely a model of the QGP. A pQCD description of jet evolution breaks down when the partonic cascade reaches energy scales around the QGP temperature, that is, $\mathcal{O}(\Lambda_{\mathrm{QCD}})$. Then, other nonperturbative effects such as thermalization and hadronization become relevant. Thermalization can be studied with QCD kinetic theory [18–20] (using an artificially big coupling), while the formation of hadrons rely on phenomenological modeling [21–23]. Alternatively, strongly coupled descriptions of parton energy loss have also been studied using the gauge/gravity duality [24–28]. While they offer a natural scenario for jet hydrodynamization in a strongly coupled plasma, the underlying quantum field theory (QFT) is not QCD, but $\mathbf{N} = 4$ Super Yang-Mills (SYM), implying the presence of large theoretical uncertainties in the extrapolation of the results to the system actually produced in heavy-ion collisions.

Due to the intricate interplay among the aforementioned effects and the multiscale nature of the process, an end-to-end analytic approach to in-medium jet evolution that matches the experimental precision is currently beyond reach. As a consequence, the theoretical interpretation of jet observables relies almost exclusively on phenomenological modeling by means of Monte Carlo (MC) event generators. Several implementations of in-medium parton showers have been proposed in the literature [13,29–38]. They differ not only in the precision in which they describe the individual ingredients of jet evolution but also in the way they assemble them. A paradigmatic example, that will be relevant in this paper, is the interleaving of vacuum and medium-induced emissions. While some approaches implement either a partial or an exact factorization between vacuum and medium-induced emissions [13,39], others include them on equal footing in their evolution equations [31,40,41]. Experimental measurements have not yet been able to pin down which is the correct approach [42–44]. Consolidating the theoretical description of in-medium jet evolution thus requires experimental guidance by means of more differential and/or precise measurements.

This paper aims to disentangle different stages of jet evolution by combining two jet substructure observables. That is, we study the angular separation between subjets as a function of their relative transverse momentum. The latter serves as an auxiliary scale that allows us to sweep through different phases of jet evolution in a controlled fashion. Our proposal strongly relies on the use of high-pt jets to ensure a clear separation between perturbative and medium-related scales. By means of state-of-the-art Monte Carlo simulations, we quantitatively address the following fundamental questions:

(1) Is there a regime of pure vacuum evolution in the in-medium development of a parton shower?
(2) Does energy loss depend on the opening angle of the splitting? If so, at which energy scale does this effect become relevant?
(3) Are elastic scatterings with the medium visible in jet substructure observables?

The underlying philosophy and technical details of the proposed observable together with its connection to previous measurements are explained in Sec. II. The concrete definition of our proposed observable is given in Sec. II B. The proton-proton baseline is studied in Sec. III including a comparison between state-of-the-art pQCD and the vacuum prediction of jet quenching event generators. Quantitative results showing the discriminating power of the proposed observable in heavy-ion collisions can be found in Sec. IV. We end up with a brief summary of our results in Sec. V. The experimental feasibility of this measurement with the upcoming runs 3 and 4 of the LHC, some analytic considerations, the impact of energy loss prescriptions and medium response, and the choice of reclustering algorithm are studied in Appendices A–E, respectively.

II. ANALYSIS STRATEGY

Our goal is to design and study an observable to probe certain corners of the radiation phase space of an in-medium jet, as sketched in a Lund-plane fashion in Fig. 1. Before entering into the precise definition of the observable, let us briefly comment on the most relevant features of this radiation phase space. All along this discussion we will assume a simplified description of the QGP. Namely, we will consider the so-called brick approximation in which the medium is static, isotropic, homogeneous, and with a fixed length L. We remark that in the Monte Carlo section, a realistic medium description will be used.

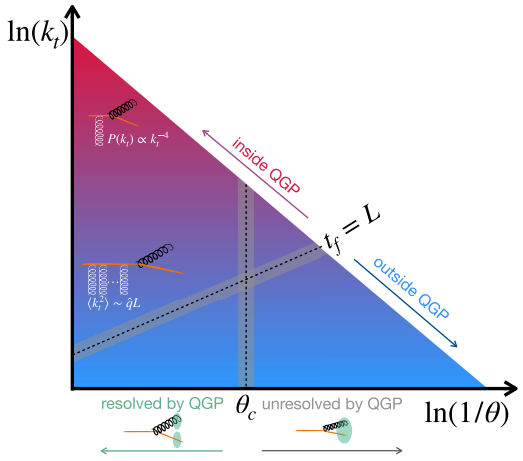

FIG. 1. Sketch depicting the different regimes of in-medium jet evolution in a Lund-plane style representation. The gray bands around $\theta = \theta_c$ and $t_f = L$ indicate that these two scales fluctuate on an event-by-event basis.

A. Brief reminder of in-medium jet evolution

For a given jet with transverse momentum p_t and cone size R, we characterize its branchings by their opening angle θ and their relative transverse momentum k_t.[1] The maximum relative transverse momentum is $k_t < p_t R$ [$\mathcal{O}(10^2)$ GeV in this study]. Another important kinematic variable is the formation time of the splitting $t_f = 2/(k_t\theta)$, which describes the quantum mechanical extent of a branching [46].

Jet constituents interact elastically and inelastically with the QGP color fields. The former results in transverse momentum broadening, while the latter induces additional radiation. Therefore, splittings in an in-medium parton shower can be either vacuumlike (i.e., described by the Altarelli-Parisi splitting function [47]) or medium-induced, with a branching probability that depends on the medium properties. For example, modeling the jet-QGP interaction in the multiple soft scattering approximation [14,15,48] results in Gaussian broadening with accumulated transverse momentum $\langle k_t^2\rangle \sim \hat{q}L$, with $\hat{q}$ the so-called quenching parameter and L the propagation length. Since the typical value of $\hat{q}$ is around 1 to 3 GeV^2/fm [49–51], elastic and inelastic medium processes mainly contribute in the soft regime ($k_t \sim \mathcal{O}(1)$ GeV) of Fig. 1. Another important feature is that these medium-induced emissions typically occur at wide angles, drifting energy out of the jet cone. Alternatively, hard collisions with the medium can occur above $\langle k_t^2\rangle > \hat{q}L$ and induce emissions with a Coulomb-like transverse momentum distribution, i.e., $\propto 1/k_t^4$ tail [16,17]. These Molière, single hit scatterings [52,53] compete with vacuumlike radiation in the high-k_t regime, although their occurrence is relatively rare for dense media.

Another medium-related scale highlighted in Fig. 1 is the decoherence angle, $\theta_c \sim (\sqrt{\hat{q}L^3})^{-1}$ [54,55]. If the opening angle of the splitting is small, the medium cannot resolve the two daughters through soft scatterings, and emissions are coherently induced on this composite, 2-parton object. Above θ_c, the daughters are resolved, and both source medium-induced radiation.

To illustrate the importance of θ_c, consider the extreme case in which the first splitting of an angular-ordered parton shower has $\theta < \theta_c$. All emissions inside the jet will be unresolved by the medium, its substructure remains unmodified, and the jet loses energy as a single object (just the initiator is quenched). In turn, when a splitting satisfies $\theta > \theta_c$, both prongs act as independent radiators of medium-induced emissions, resulting in a larger energy loss. This angular dependence of energy loss translates into a sizeable modification of jet substructure observables by means of a selection bias, or survivor bias effect. Due to the presence of a steeply falling jet p_t spectrum, inclusive jet ensembles at any given p_t in heavy-ion collisions will be dominated by those jets that on average lost the least amount of energy. Therefore, the number of jets with wide-angle substructure, $\theta > \theta_c$, is suppressed compared to proton-proton collisions in any inclusive jet observable where unavoidably minimum jet p_t thresholds are imposed [56–61].[2]

An important observation is that varying the jet reconstruction parameters, (p_t, R), enables the separation of medium dynamics from vacuum physics. For example, raising the jet p_t increases the phase space for high-energy emissions (i.e., the upper diagonal of the emission phase space in Fig. 1 moves to higher values). Since $\hat{q}$ depends only mildly on energy [67,68], the scale at which medium-induced emissions dominate ($k_t^2 \sim \hat{q}L$) will remain the same and the new phase-space region should be mainly populated by vacuum emissions. Similarly, increasing the jet radius R further separates the $\theta = R$ boundary from the θ_c scale (again almost independent of the jet energy). We will exploit these facts in the definition of our observable.

B. Observable definition

We cluster events with the anti-k_t algorithm [69,70] using a jet radius of $R = 0.2$ and select all jets that satisfy $p_t > 400$ GeV, and $|\eta| < 2.8$. This subset of jets is then reclustered with the Cambridge/Aachen algorithm (C/A) [71,72], effectively reordering the branching history in decreasing angles.[3] For each of these jets, we find the hardest splitting, i.e., the splitting with maximum $k_t = \min(p_{t1}, p_{t2})\theta$. If the splitting satisfies $k_t > k_t^{\min}$, we record the opening angle of this hardest branching, which we denote θ_{hard}.

Let us now justify each of the choices that we have made in the previous paragraph and comment on their experimental feasibility:

(1) $R = 0.2$: there are certain advantages of using jets with small cone sizes. The physics associated with vacuumlike emissions and coherence that we are interested in the present work typically appear at

[1]We follow the standard Lund jet plane definitions, $\theta = \sqrt{(y_1 - y_2)^2 + (\phi_1 - \phi_2)^2}$, $k_t = \min(p_{t1}, p_{t2})\theta$, where the two prongs of the splitting are denoted with subscripts 1 and 2 [45].

[2]Selection biases are also present even if energy loss is independent of the jet substructure. For example, gluon jets are more suppressed since, on average, they lose more energy than quark jets due to their larger color factor. As gluon jets are typically wider, this bias would also cause some narrowing of the final quenched jet ensemble. This is sometimes referred to as a bias in the q/g fraction [62–64]. Additionally, the selection bias mixed with color resolution (i.e., small angle splittings do not source energy loss) gives even stronger narrowing and it is necessary to explain jet measurements [39,61,65,66].

[3]We explore different choices for the reclustering algorithm in Appendix E.

small angles (< 0.1). The reduced jet area decreases the contamination from the uncorrelated fluctuating background and notably improves experimental systematic uncertainties. Moreover, smaller jet cones also reduce the contribution from medium response, which typically populates the larger angle region, thus further improving the signal.

(2) $p_t > 400$ GeV: the larger the jet p_t is, the more pQCD dominated the observable is. This guarantees not only calculability but also a large separation of scales, breaking up the problem of in-medium jet evolution into simpler pieces. Going to higher momenta, however, significantly reduces the statistics. The expected number of jets in PbPb collisions during runs 3 and 4 at the LHC is discussed in Appendix A.

(3) $k_t^{\min}$: this auxiliary variable is central to our approach. Its role is to slice the radiation phase space, separating different regimes of jet evolution. We explore three values: 20, 5, and 1 GeV. The highest $k_t^{\min}$ selects splittings at the top of the emission phase space (Fig. 1), with formation times less than 0.4 fm, and addresses the question of whether vacuum splittings indeed dominate the early evolution of jets. In the multiple soft scatterings approximation, medium-induced emissions will typically appear at $k_t^2 \approx \hat{q}L \approx 2^2$ GeV^2 and $\theta > \theta_c$. Therefore, if the value of the cut is large enough $k_t^{\min} \gg \sqrt{\hat{q}L}$, one expects a vacuumlike substructure even in the medium. We refer to this as the factorization (or separation) of vacuumlike and medium physics. Lowering $k_t^{\min}$ (but still keeping it far from nonperturbative scales $\mathcal{O}(1)$ GeV) opens up the phase space for perturbative collinear splittings below θ_c, and the observable becomes sensitive to splittings being resolved or unresolved by the medium. In addition, it could potentially be affected by perturbative elastic scatterings and medium-induced emissions, whose modeling changes in different jet quenching models. Finally, the lowest value of $k_t^{\min}$ maps the region dominated by nonperturbative physics.

(4) θ_{hard}: the angular distribution of the hardest splitting is known to be sensitive to the substructure dependence of energy loss [65], e.g., as caused by θ_c [54,73]. It is also motivated by the simplified theoretical picture in which jet energy loss depends on an angular resolution scale, namely θ_c [54,73]. From the point of view of distinguishing vacuum from medium-induced emissions, this choice is also reasonable since the latter typically occur at large angles as a result of transverse momentum broadening.

In the landscape of other jet substructure studies, the proposed algorithm is unique in the sense that it first selects the hardest splitting above the $k_t^{\min}$ cut and then studies its angular distribution. The main difference with respect to *dynamical grooming* observables with $a = 1$ [74] is precisely $k_t^{\min}$. Predictions for dynamically groomed observables in heavy-ion collisions have been put forward in Refs. [65,75,76], demonstrating its sensitivity to color coherence. Given our interest in studying the earliest stages of the shower, selecting the splitting with the shortest formation time might *a priori* be appealing [74,77,78]. Nevertheless, these splittings can have an arbitrarily low k_t, and therefore the observable is polluted with nonperturbative corrections. Including a transverse momentum cut was also explored in the *Late-k_t* approach [79], where instead of the hardest, the most collinear splitting above a certain $k_t^{\min}$ is selected. This option is not well suited for our purposes since we want to explore the full angular distribution. Furthermore, *SoftDrop* [80] with $\beta = 1$ and $z_{\text{cut}} = k_t^{\min}/(p_t R)$ would probe the same phase space as we do, but it also biases the angular information by selecting the widest instead of the hardest splitting. So far, the SoftDrop setup mostly explored in heavy-ion collisions considers $\beta = 0$ [66,76,81–87]. Setting $\beta = 0$ does not restrict the k_t of branchings and, therefore, nonperturbative effects might still be sizeable. Instead of selecting the hardest splitting per jet, one could choose all primary splittings with $k_t > k_t^{\min}$, corresponding to a slice of the *primary jet Lund plane* [45,88]. This option would explore all the physics mechanisms we are interested in but, for the sake of simplicity, we stick to the one-splitting-per-jet case. Finally, resolution effects on *energy correlators* are also currently under study [89,90].

III. PROTON-PROTON BASELINE

We begin our analysis by exploring the behavior of the observable in proton-proton collisions at $\sqrt{s} = 5.02$ TeV. In Fig. 2, we show the self-normalized θ_{hard} distribution for different values of $k_t^{\min}$ as obtained by matching, in a Powheg approach [91], the exact $pp \to jj$ next-to-leading order (NLO) matrix element to the PYTHIA8 parton shower [92]. We observe a clear shift towards smaller angles when decreasing $k_t^{\min}$. This feature can be easily understood from Fig. 1, since phase space in the collinear regime opens up when lowering the $k_t^{\min}$ constraint. The lowest accessible angle is given by $\theta_{\text{hard}}^{\min} \propto k_t^{\min}/p_t$.[4] We anticipate that the net angular reach for a given $k_t^{\min}$ will be an important aspect when including medium effects. On the wide-angle side, we note that angles larger than R are possible due to the C/A reclustering, but they are highly unlikely. The error bands correspond to statistical uncertainties only (combined in the ratio plots).

[4]Notice that our jet selection is $p_t > 400$ GeV, and therefore there is no hard cutoff on the smallest angle.

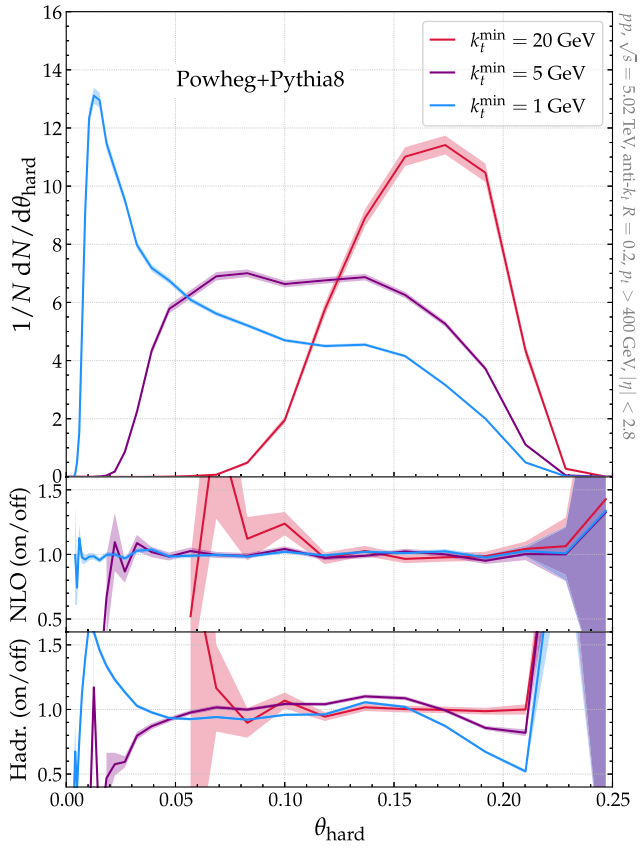

FIG. 2. The angular distribution of the hardest-k_t splitting inside inclusive, pp jets for different $k_t^{\min}$ values in NLO POWHEG+PYTHIA8. The bottom panels show (i) the impact of NLO matching and (ii) the impact of hadronization on the pure shower samples, i.e., not matched to NLO. In all cases, the band represents the statistical uncertainty.

In the lower panels of Fig. 2 we quantify the impact of NLO corrections and hadronization.[5,6] The former is expected to be more relevant for the largest $k_t^{\min}$ since, in that regime, the true matrix element notably differs from the soft-and-collinear approximation used by the parton shower. Indeed, we observe that for $k_t^{\min} = 1$, 5 GeV, NLO corrections are practically irrelevant. In turn, we find a moderate effect of about 20% for $k_t^{\min} = 20$ GeV.

Hadronization effects have the opposite $k_t^{\min}$ dependence compared to NLO corrections. The deeper we go into the infrared regime by lowering $k_t^{\min}$, the bigger the corrections are. For $k_t^{\min} = 20$ GeV we find that hadron and parton curves agree within statistical uncertainty (except in the $\theta_{\rm hard} > R$ region coming from hadrons on the boundary of the jet cone), thus demonstrating the pQCD purity of this region of phase space. The intermediate value of $k_t^{\min}$ receives less than 20% hadronization corrections in a wide angular region, while they reach up to 50% for $k_t^{\min} = 1$ GeV.

Next, we compare these state-of-the-art pQCD results with the pp (i.e., vacuum) baseline of the jet quenching Monte Carlo codes that we use in this paper: HYBRID [36], JetMed [13,95], and JEWEL [30,41]. This comparison is relevant since none of the current jet-quenching MCs implement NLO corrections. It could be argued that deficiencies in vacuum modeling are irrelevant since they would potentially cancel in a medium-to-vacuum ratio. However, this statement is exact only when vacuum and medium physics are entirely decoupled. This is actually not the case in most jet-quenching Monte Carlo event generators. A deficient description of the pp baseline can lead to a misleading interpretation of the medium-modified distributions. The models under comparison have different vacuum showers: HYBRID is built on the default tune of PYTHIA8.3, while JEWEL implements a virtuality-ordered PYTHIA6-like shower [96]. They both include initial-state radiation and hadronization, in contrast to JetMed, which relies on a pure final-state shower at parton level and thus misses many ingredients that might be particularly relevant at low p_t and large jet radii. The three models are compared in Fig. 3 for all values of $k_t^{\min}$. For the highest k_t cut we observe quite a good agreement ($< 10\%$ differences) among the three models. Remarkably, we also find the ratios to the state-of-the-art vacuum baseline to be compatible with unity in the whole angular range, although statistical uncertainties blow up in the edge bins. The fact that the parton-level curve obtained with JetMed agrees with the rest in the bulk of the distribution indicates that the observable is indeed dominated by pQCD physics. This well-defined vacuum baseline is an essential requirement to unambiguously identify medium modifications. For the $k_t^{\min} = 5$ GeV setup, JetMed and JEWEL deviate up to 25% in the $\theta_{\rm hard} < 0.05$ region from the POWHEG+PYTHIA8 baseline. It is important to keep in mind that this regime of very small angles will play a role in the medium studies. This consensus among models breaks down when $k_{t,\rm min} = 1$ GeV. The 50% disagreement in the JetMed case is mainly caused by the lack of hadronization, as we show in Fig. 2. Naturally, the HYBRID model ratio to NLO + Pythia8 is compatible with 1 since they share the same shower and, in this regime, NLO corrections are negligible. The PYTHIA6 vs PYTHIA8.3 differences result in an up to 20% deviation in the JEWEL case.

After this detailed analysis of the pp baseline in which we have found a remarkably good agreement between Monte Carlo codes for the highest $k_t^{\min}$ values, we proceed to study medium modifications.

[5]We also performed NLO studies with MadGraph5_aMC@NLO +HERWIG [93,94], resulting in similar curves, although with a slower statistical convergence.

[6]Multiparton interaction effects were also studied and they are negligible.

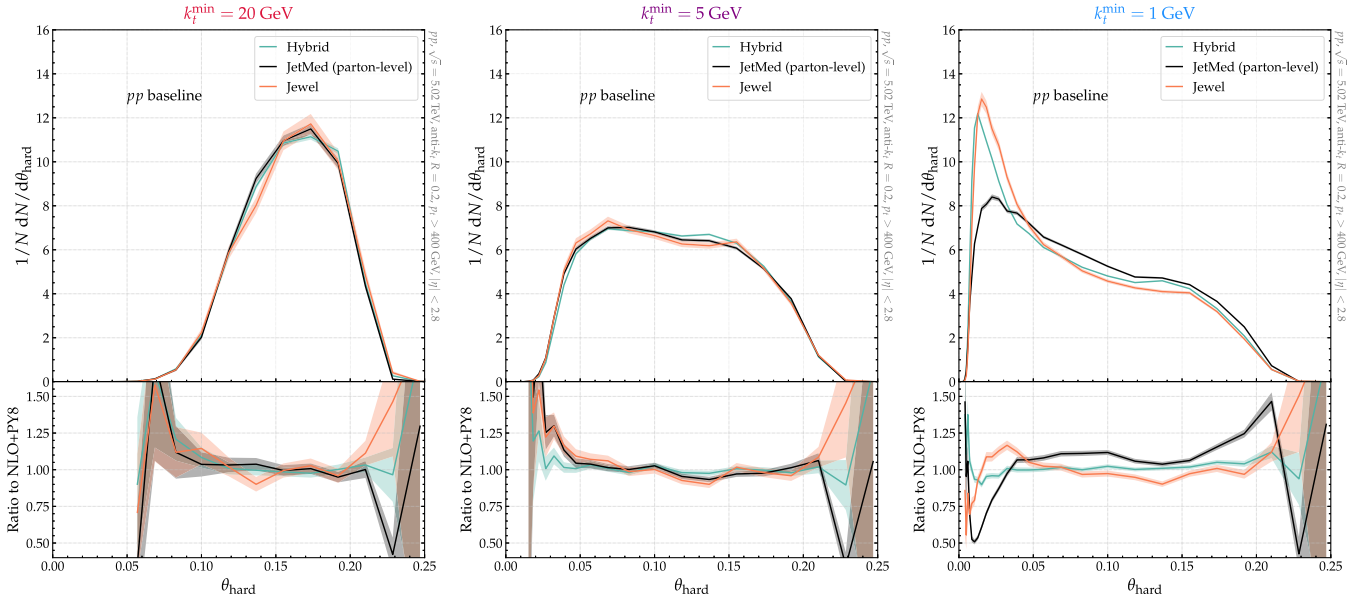

FIG. 3. The pp baseline prediction for θ_{hard} by different jet quenching Monte Carlo simulations. From right to left the value of $k_t^{\min}$ decreases. The bottom panel displays the ratio to the state-of-the-art prediction, namely POWHEG+PYTHIA8.

IV. HEAVY-ION RESULTS

In this section we apply our analysis technique for jets in heavy-ion collisions, using some of the most popular jet quenching models. We demonstrate the advantage of slicing the jet substructure by isolating different effects in the medium one by one. These MC studies employ a high number of jets to better illustrate the physics under study. A discussion on the projected experimental statistics and its uncertainties can be found in Appendix A.

A. Radiation phase space for MCs under study

To gain intuition on the medium modifications to the θ_{hard}-observable shown below, we first simulate the analog of Fig. 1 with the three jet-quenching Monte Carlo codes introduced in the previous section: JetMed, HYBRID, and JEWEL. That is, we plot in Fig. 4 the PbPb-to-pp ratio of the $(k_t, \theta_{\mathrm{hard}})$ self-normalized density of the hardest splitting within our jet selection. Let us discuss each of the three plots individually and, in particular, the relevant scales therein:

(1) JetMed [13,95]. The description of the QGP in this model is rather simplified, i.e., it can either run with a Björken expanding media [97] or a brick. This paper uses the latter with fixed path length $L = 4$ fm and $\hat{q} = 1.5\ \mathrm{GeV}^2/\mathrm{fm}$. The parton-medium interaction is calculated in the multiple soft scatterings approximation. An explicit realization of color coherence dynamics is implemented employing θ_c (with a constant value event by event). The typical relative transverse momentum of induced emissions is $\langle k_t \rangle = \sqrt{\hat{q}L} \approx 2.4$ GeV, and they appear above

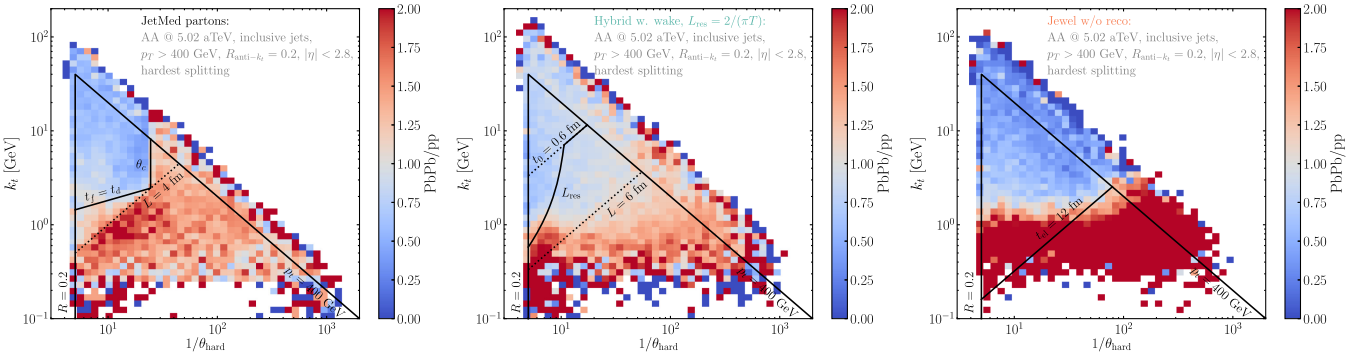

FIG. 4. 2D distribution of the hardest splitting $(\theta_{\mathrm{hard}}, k_{t,\mathrm{hard}})$, using different jet-quenching models (similar to the sketch in Fig. 1). The ratio to pp illustrates the modification of jets inside the quark-gluon plasma. The approximated resolution phase spaces are denoted with black lines. Note that the ratio extends in the upper diagonal because of our $p_t > 400$ GeV selection.

the critical angle $\theta > \theta_c = 2/\sqrt{\hat{q}L^3} = 0.04$. These induced emissions are responsible for the small enhancement below the $t_f = t_d = [4/(\hat{q}\theta^2)]^{1/3}$ line.[7] The most prominent feature in Fig. 4 is the depletion of emissions in the polygon delimited by the $t_f < t_d$ and $\theta > \theta_c$ boundaries. Vacuumlike emissions in this corner of phase space are resolved by the medium and source more energy loss. Due to the selection bias (described in Sec. II) these wide-angle substructure jets are thus suppressed. Another relevant feature of this model is that vacuumlike emissions are forbidden (vetoed) in the $t_d < t_f < L$ region since this is the regime dominated by broadening dynamics and not enhanced by the jet energy. In this context, vacuum and medium-induced cascades do factorize exactly, with the former acting as sources for the latter. Finally, a third stage of vacuumlike showering is also implemented with an extended angular region, i.e., the first emission outside the medium can be emitted at any angle due to the color randomization suffered by the emitting dipoles during their evolution throughout the medium [73]. This third stage of the shower fills the lowermost part of the phase space, down to 1 GeV. The hard-coded value of θ_c helps to quantify the sensitivity of the $\theta_{\rm hard}$ observable to coherent vs incoherent energy loss. Finally, no medium response and hadronization are implemented in JetMed.

(2) HYBRID [36,98]. This model runs a perturbative vacuum shower down to the hadronization scale and then rewinds through the branching history to incorporate an energy loss rate computed at strong coupling [28,99]. No medium-induced emissions are considered. The total amount of energy lost by splittings depends on their propagation distance within the QGP, as determined by embedding the PYTHIA8 event in a realistic heavy-ion simulation using 2 + 1D viscous hydrodynamics [100]. Event-averaged hydro profile was used with 0–5% centrality and the freeze-out temperature of 145 MeV. The jet production points are sampled from two overlapped nuclear density profiles using the Glauber model [101]. Emissions whose formation time is smaller than the hydrodynamic initialization time $t_0 = 0.6$ fm or longer than the freeze-out are not quenched. Another feature of the HYBRID model is that only those partons that are "separated enough," i.e., resolved by the medium, lose energy independently. The medium-resolution power is controlled by the $L_{\rm res}$ parameter, which depends on medium properties such as the local temperature and therefore it fluctuates for every parton [102]. For two color-connected legs to lose energy independently, their transverse distance, $r_{\perp,\rm dip} \approx \theta(L - t_f)$, has to be larger than the resolution length $L_{\rm res}$. In what follows, we choose $L_{\rm res} = 2/(\pi T)$ by default and explore other values of $L_{\rm res}$ in Appendix C. To illustrate the resolved phase space, we pick a representative value of the medium length in central PbPb collisions, $L \sim 6$ fm, and $L_{\rm res} = 2/(\pi \cdot 0.25[\text{GeV}]) \approx 0.5$ fm. All emissions above the $r_{\perp,\rm dip} = (L - t_f)\theta > L_{\rm res}$ (black curve in Fig. 4) are resolved by the medium, lose more energy, and are therefore suppressed by the selection bias. Here, the phase space boundary is not as sharp as for JetMed because both L and $L_{\rm res}(T)$ fluctuate. The lost energy is then hydrodynamized, producing jet-induced wakes that decay into hadrons at the freeze-out hypersurface of the flowing medium [103]. These wake particles get clustered with the jet resulting in an excess of soft, wide-angle splittings (lower left corner in Fig. 4). All results shown below include medium response and a detailed study of its impact is presented in Appendix D. Note that we don't include in our analysis particles coming from the hydrodynamical evolution that did not interact with the jet. These particles correspond to the so-called uncorrelated background that is typically removed by background subtraction methods (see Appendix A for more details).

(3) JEWEL [30,41]. The medium in JEWEL is modeled as a thermal, longitudinally expanding parton gas in which PYTHIA6-like scatterings are embedded according to a Glauber sampling similar to the HYBRID model. The propagating partons can either emit vacuum radiation or undergo elastic (2-2) scatterings with medium partons at each evolution step. The process with the shorter "time" (formation time, or virtuality, compared to light-cone time) is realized. Elastic scatterings result in transverse momentum broadening, drifting energy out of the jet cone, and causing energy loss. Scatterings also reset the shower scale and induce collinear emissions without changing the jet energy. To estimate at which time ($t_{\rm el}$) elastic scatterings become dominant, we compare the scattering probability $p_{\rm el} \approx (t_{\rm el} - t_0)/l_{\rm mfp}$ with the radiation one $p_{\rm rad} \approx \int_{t_0}^{t_{\rm el}} dt \int_0^1 dz P_{1\to2}(t,z)$. Here, $l_{\rm mfp}$ is the average distance between scatterings, t_0 is the initial formation time, and the splitting probability (expressed with formation time) is $P_{1\to2} \approx \alpha_s P(z)/(\pi t)$, where we used the Altarelli-Parisi splitting function $P(z) \approx 2C_i/z$. When $t \gg t_{\rm el}$, elastic scatterings interrupt vacuum radiation and induce extra collinear emissions (small angle, hard enhancement, $z \sim 1$ in Fig. 4). Additionally, elastic scatterings broaden soft splittings to wider angles

[7]The decoherence time t_d is the time at which a color-connected dipole gets resolved by the medium, by destroying its color correlation via multiple color rotations.

(wide angle enhancement below 1 GeV in Fig. 4).[8] In contrast to the previous two models, an additional notion of color coherence is not implemented. The medium response is accounted for by keeping track of the recoiled medium partons after an elastic scattering takes place. These recoilers however free stream without further scatterings or radiation. In what follows we will disregard recoil particles and explore their impact in Appendix D. We do this as our current setup of JEWEL would overestimate all medium response effects since, after the scattering, their evolution is frozen, i.e., they are nondynamical.

We would like to note that one of the key questions that our paper wants to address is whether the proposed observable is more sensitive to the medium evolution than to the parton shower implementation. As we will see, the fact that all three models result into qualitatively similar trends despite their radically different medium evolution descriptions points toward a clear sensitivity to the parton shower. This has already been observed in other substructure measurements that are compatible, within uncertainties, to various implementations of medium dynamics, e.g., JEWEL VS HYBRID (see e.g., Refs. [42–44]).

B. Early times/vacuum-dominated regime

We first study jets in PbPb collisions whose hardest splitting satisfies $k_t > 20$ GeV. This region corresponds to very short formation times, i.e., parametrically $t_f < 2p_t/(k_t^{\min})^2 \approx 0.4$ fm, smaller than the mean free path $l_{\rm mfp} = (\rho\sigma_{\rm el})^{-1}$ (where ρ is the density of scattering centers and $\sigma_{\rm el}$ the total elastic cross section). The $\theta_{\rm hard}$ distribution is displayed in Fig. 5. We observe that all models agree within statistical uncertainties and that the medium-to-vacuum ratio is remarkably close to unity.[9] This result suggests that, in this upper corner of phase space, vacuum-like splittings are likely to be tagged and that its prongs lose the same amount of energy, independently of their opening angle. We show this independence analytically in Appendix B. We refer to this as the factorization (or separation) of vacuum and medium-induced physics. This separation is very general in the sense that it is independent of the medium modelling when one goes to asymptotically high jet-p_t and $k_t^{\min}$. In the JetMed context, these results are easily interpreted since the cut excludes the possibility of tagging medium-induced emissions ($k_t^{\min} \gg \sqrt{\hat{q}L}$) and $\theta_{\rm hard}$ is always bigger than θ_c. We would like to note that HYBRID wake effects at $k^{\min} = 20$ GeV are completely negligible, and recoil particles in JEWEL are strongly suppressed (see in Appendix D).

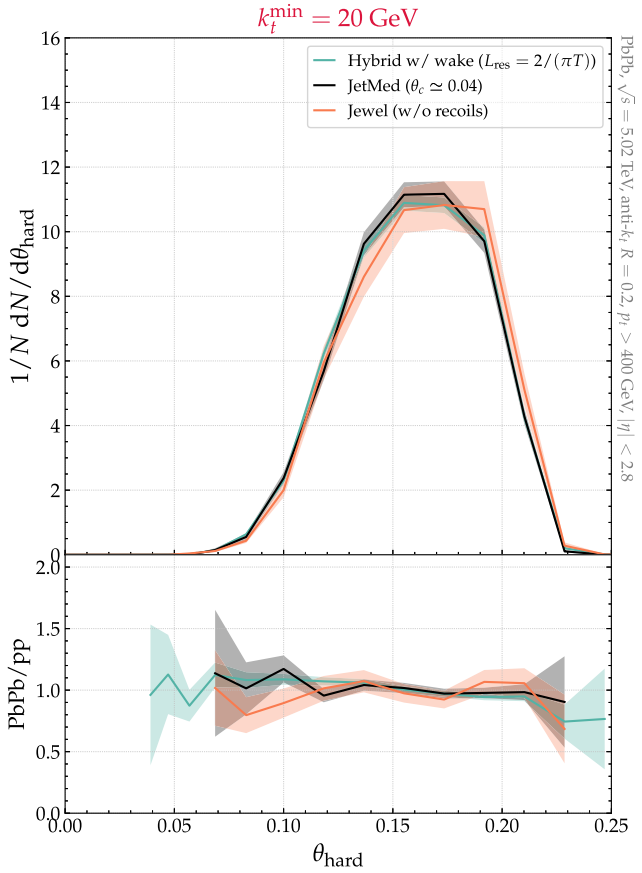

FIG. 5. The angular distribution of the hardest-k_t splitting inside inclusive jets in heavy-ion collisions with $k_t^{\min} = 20$ GeV for the jet quenching Monte Carlo event generators described in Fig. 4. The bottom panel displays the medium-to-vacuum ratio.

We would like to highlight that not all jet-quenching models predict a flat ratio. For example, a potential source of substructure modifications at such high energy scales is the single-hit (or higher-twist) corrections induced by rare, hard interactions with the medium. These hard interactions modify both the elastic scattering probability (i.e., lead to Moliere scatterings) and the spectrum of induced radiation. The former is included in JEWEL, while the latter is in the focus of the SCET$_g$ formalism [104] and MATTER + LBT Monte Carlo generator [34,35]. However, the latest implementation of MATTER makes use of a virtuality-dependent $\hat{q}$ [39,105] that effectively reduces the impact of such corrections in this high-k_t regime.

The experimental measurement of the proposed observable has the potential to unambiguously establish whether vacuum physics dominates the early stages of jets in heavy-ion collisions. Knowing that there is a region of phase space dominated by vacuum splittings implies that all jet quenching models should agree not only among them, but also

[8]In Fig. 4, induced collinear emissions and broadening overlap. In our numerical tests, we however identified the separation of these two regions.

[9]Note that these distributions are self-normalized and thus the overall suppression of the jet spectrum is factored out. This choice is justified since our main interest is a potential shape modification.

with the pp baseline, within that given region. This would represent a major step forward in our understanding of jet quenching and is one of the main results of this paper.

C. Substructure-dependent energy loss

When lowering the cut to $k_t^{\min} = 5$ GeV, we enter a domain where one can test the substructure dependence of energy loss. Here, emissions with much longer formation times $\lambda_{\rm mfp} \ll t_f < 6.4$ fm appear, while soft medium-induced splittings are still suppressed $k_t^{\min} > \sqrt{\hat{q}L} \approx 2.4$ GeV. In the color coherence picture sketched in Fig. 1, we expect splittings with $\theta < \theta_c$ to appear, which are unresolved by the medium. As we have discussed, jets with wider splittings $\theta > \theta_c$ lose more energy and are suppressed due to selection bias. Consequently, we expect the suppression of $\theta_{\rm hard} > \theta_c$ (or equivalently an enhancement of $\theta_{\rm hard} < \theta_c$). Most modern jet quenching models implement this coherence (or resolution) effect, but they differ in the shape of the phase space boundary as discussed in Sec. IV A (see in Fig. 4). Theoretically, this boundary is not known beyond the soft-and-collinear limit, and models implement it differently. An experimental measurement in this regime, therefore, could put tighter constraints on the modeling of the resolution phase space.

In Fig. 6, we show the angular distribution of the hardest splitting $\theta_{\rm hard}$ for $k_t^{\min} = 5$ GeV. The PbPb-to-pp ratio in JetMed displays a sharp enhancement at $\theta_c = 0.04$, a clear consequence of color resolution and selection bias. Our expectation is that, on both sides of θ_c, the jet substructure does not change much, it is still vacuumlike (the ratio is flat). For the HYBRID model, the resolution boundary is not as sharp as it gets washed out due to fluctuations in the propagation length, temperature, and parton energy. The overall picture is however similar to JetMed: wide-angle splittings are suppressed. Results for the HYBRID model with different $L_{\rm res}$ values are shown in Appendix C. We would like to highlight that the angular distribution in the $L_{\rm res} = \infty$ fully coherent limit of the HYBRID model (only the initiator loses energy independent of the substructure) is barely modified as compared to vacuum, as expected. Even though the wake is included in Fig. 6, the 5 GeV cut is still large enough to completely remove its effects (see it in more detail in Appendix D).

The JEWEL model is somewhat distinct from the other two models since it lacks an explicit implementation of color coherence. The competition between elastic scattering and vacuum radiation still outlines a boundary that we referred to as $t_{\rm el}$. However, this boundary is beyond the phase space limited by $k_t^{\min} = 5$ GeV (see Fig. 4) and therefore the medium-to-vacuum ratio is compatible with unity. Jets in JEWEL of course lose energy, but their internal structure is vacuumlike even at $k_t \sim 5$ GeV. This ratio mildly changes when keeping track of the recoiling partons as we present in Appendix D.

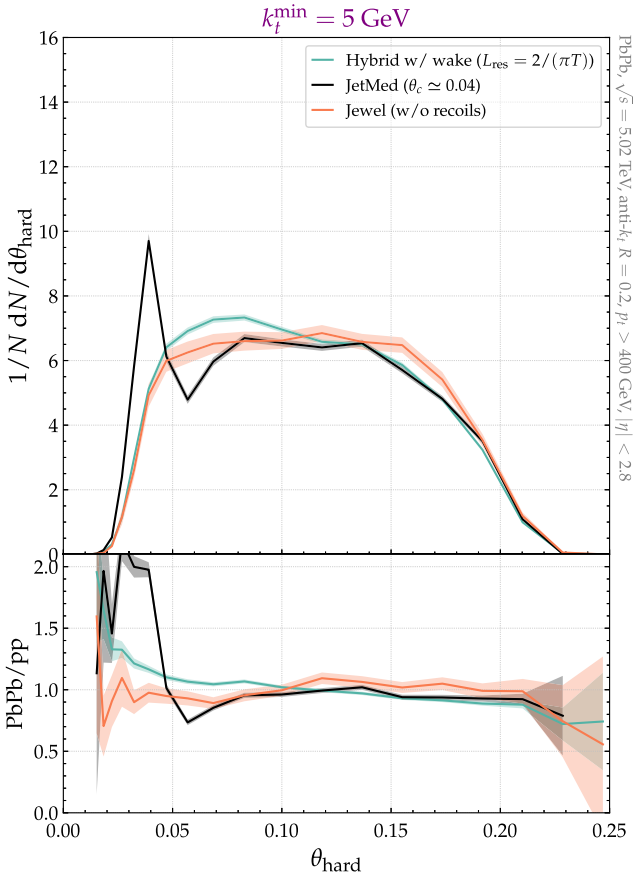

FIG. 6. Same as Fig. 5 but for $k_t^{\min} = 5$ GeV.

Let us reemphasize that the proposed measurement, after identifying the vacuumlike dominated region of phase space, has the potential to pin down the angular dependence of energy loss. In particular, it can quantify the angular resolution power of the QGP, tightly connected with its microscopic, transport properties, while putting tighter constraints on the actual size of the resolved phase space.

Furthermore, at wider angles ($\theta_{\rm hard} \gg \theta_c$) our observable with $k_t^{\min} = 5$ GeV is sensitive to the presence of hard recoils produced in perturbative elastic scatterings (also referred to as Molière scatterings), while remaining insensitive to the presence of the soft hadrons from the jet-induced wake (see the detailed study in Appendix D). This fact exemplifies the discriminating power of future experimental measurements of this observable to distinguish between different physical assumptions on the thermalization dynamics of jets in the QGP.

D. Nonperturbative regime

As a last step, we set a lower selection cutoff $k_t^{\min} = 1$ GeV. By doing this, we extend the low-angle reach of the distributions and we also enter a region where contributions from non-perturbative effects are expected. In addition, as discussed in Appendix A, fake splittings might

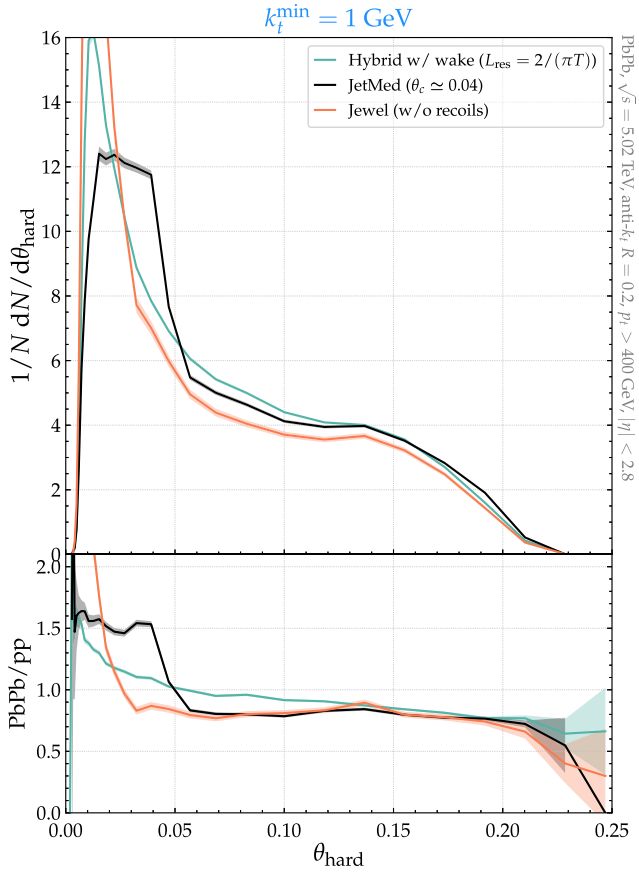

FIG. 7. Same as Fig. 5 but for $k_t^{\min} = 1$ GeV.

hamper the unfolding of experimental results. Even if it might not be possible to produce particle-level measurements in experiments, we think it is important to show when and how the perturbative picture studied above breaks down. The results are shown in Fig. 7. With the extended low-angle reach, the threshold behavior of the JetMed distribution at $\theta_{\rm hard} = \theta_c$ becomes more apparent. The ratio on both sides of θ_c is flat, showing the dominance of vacuumlike substructure. The contribution of medium-induced emissions seems to be subleading (recall that $k_t^{\min} < \sqrt{\hat{q}L} = 2.4$ GeV). An important caveat is that hadronization corrections can reach up to 50% in this regime (see Fig. 3) and thus JetMed might not be accurate in this regime.[10]

[10]It is often argued that hadronization effects cancel in the PbPb-to-pp ratio. This is, however, a model-dependent statement that we have explicitly checked by computing the double ratio between the PbPb and pp distributions at hadron and parton levels. In the HYBRID model, this ratio is consistent with unity for this value of $k_t^{\min}$, while in JEWEL $\mathcal{O}(1)$ hadronization effects are observed for $\theta < 0.05$. This difference originates from the fact that only JEWEL changes the number of partons that undergo string fragmentation, while HYBRID either reduces their energy or removes them completely.

For the HYBRID model, the narrowing of the distribution persists, which indicates that wake particles, typically manifesting as a bump at large angles (see Appendix D), are suppressed by this observable with this set of fiducial cuts, mainly due to the small $R = 0.2$ choice. We note that the fact that JetMed and HYBRID ratio curves cross unity at the same angle is coincidental. In fact, while the JetMed curves switch from depletion to enhancement at $\theta_{\rm hard} \sim \theta_c$ for $k_t^{\min} = 1 \to 5$ GeV, the crossing point in the HYBRID case changes from $\theta_{\rm hard} \sim 0.1$ to 0.05 when lowering $k_t^{\min}$ from $5 \to 1$ GeV. Thus, with a high enough angular resolution, the experimental measurement of the crossing point as a function of $k_t^{\min}$ could potentially disentangle between selection bias effects. Differentiating in centrality and jet p_t would further prove the existence of a critical resolution angle.

In the case of JEWEL, we also observe an enhancement of narrow structures in PbPb versus pp. As we previously discussed, we attribute this to elastic scatterings, which reset the vacuum shower scale inducing collinear emissions. Further elastic scatterings did not broaden these emissions enough towards wider angles. All three models indicate that, even in this low domain of $k_t^{\min}$, the prevailing medium modification of the $\theta_{\rm hard}$ distribution is the intrajet structure dependence of energy loss.

It is worth noting that this distribution is significantly altered when introducing recoil effects in JEWEL (see Fig. 11). At the same time, it turns out to be remarkably resilient to wake particles. One can still study the wake particles and therefore the thermalization of jets by opening the jet cone to $R = 0.4$ (and keeping $k_t^{\min} = 1$ GeV), see in Appendix D.

V. SUMMARY

This study proposes a novel analysis strategy aiming at experimentally accessing different stages of jet evolution in heavy-ion collisions. It explores the angular distribution of the hardest splitting, $\theta_{\rm hard}$, above a transverse momentum threshold $k_t^{\min}$. This momentum scale can be tuned so as to enhance or suppress certain features of jet dynamics. For example, selecting hard enough splittings ($k_t^{\min} \sim 20$ GeV) the observable is dominated by perturbative physics and, in particular, by the vacuum evolution of an in-medium jet. This perturbative region extends to even lower cuts (~5 GeV) with the additional sensitivity to the color resolution power of the medium and hard elastic scatterings. In contrast, when the hardest splitting becomes commensurate to the QGP and confinement scales ($k_t^{\min} \sim \Lambda_{\rm QCD}, T$), it becomes sensitive to thermalization and hadronization effects in the medium. A key observation is that this strategy is optimal when the jet radiation phase space is so large ($p_t^{\rm jet} = \mathcal{O}(100)$ GeV) that it admits well-separated regions between vacuum- and medium-dominated dynamics. Although the outlined strategy is

completely general/data driven, we illustrate the potential of this observable by using three of the most popular jet quenching Monte Carlo event generators: HYBRID, JetMed, and JEWEL. First, we performed a systematic study of the proton-proton baseline using state-of-the-art techniques (POWHEG+PYTHIA8). We compared this baseline to the vacuum prediction of jet-quenching event generators. At sufficiently high $k_t^{\min}$ cut, we find remarkably good agreement among all vacuum models, and therefore any potential modifications due to medium effects arise from a well-controlled baseline. Differences in the vacuum mode of the jet-quenching models gradually appear at low k_t, where hadronization corrections become sizeable (up to 50% for $k_t^{\min} = 1$ GeV).

On the heavy-ion side, we first address the question of whether the early stages of in-medium evolution are dominated by vacuum dynamics. To that end, we selected $k_t^{\min} = 20$ GeV, which is high enough to ensure perturbativity. The three models under study predict a PbPb-to-pp ratio compatible with unity across all θ_{hard} values. We interpret this as the result of a vacuumlike splitting being tagged, followed by energy loss that is largely independent of the substructure. We show analytically why the amount of lost energy is independent of the opening angle of the splitting in this hard regime. An experimental confirmation of this high $k_t^{\min}$ result will show, for the first time, a vacuum-dominated observable in a heavy-ion environment.

Next, we extend the angular coverage of the observable by lowering to $k_t^{\min} = 5$ GeV. This intermediate value opens up the possibility of understanding the small-angle dependence of energy loss while staying in the perturbative regime. At small angles, a reduction of energy loss is expected due to color resolution effects. This angular dependence is then enhanced by selection bias effects, where the jet ensemble contains fewer jets with wider substructure, as they typically lose more energy than narrower ones.[11] We indeed observe a clear narrowing in the θ_{hard} distribution in those models where some sort of resolution scale is implemented. In regards to wide-angle enhancement, we observe the imprints of hard elastic scatterings, especially for wider $R = 0.4$ jets, in JEWEL. For the HYBRID model, there is no signal from the medium response as the implemented thermal wake is removed by the $k_t^{\min} = 5$ GeV cut. The experimental test of this intermediate $k_t^{\min}$ result could reveal the color resolution scale in the medium, a fundamental property of the QGP. Furthermore, this region also gives experimental access to explore hard (Molière-like) elastic scatterings in the medium.

Decoupling selection bias and color coherence effects might be possible with high enough experimental precision or with complementary measurements in γ/Z+jet events [59,106], at forward rapidities [61] or by means of a centrality scan [107]. In fact, recent experimental results from CMS in $\gamma +$ jet events have shown that the selection bias can be suppressed by reducing $x_J = p_{t,\text{jet}}/p_{t,\gamma}$ [44]. We leave the study of the θ_{hard} observable in boson-tagged events for future work.

Finally, we explore the scenario in which $k_t^{\min} = 1$ GeV, which lies in the nonperturbative regime. We find that in JetMed the θ_{hard} distribution is narrowed in PbPb due to the color resolution with selection bias effects and only a few medium-induced emissions get tagged for narrow jets ($R = 0.2$). This spoils the possibility of measuring the medium-induced emission kernel with this observable and endorses the idea of doing so by exploring a regime in which vacuumlike emissions are strongly suppressed, such as the dead cone [79,108,109]. Another effect that this value of $k_t^{\min}$ targets is the soft medium response, i.e., jet thermalization. Wake particles in the HYBRID model leave a weak imprint on this observable mainly due to the use of relatively narrow $R = 0.2$ jets. In the JEWEL case, recoil medium particles create a broadening of the θ_{hard} distribution around the jet boundary. This regime, although experimentally challenging to unfold, has the strongest potential to help us understand jet thermalization and constrain the modeling of medium response in jet-quenching Monte Carlo generators.

As future steps, we will work on the analytic calculation of this observable in proton-proton collisions at high-logarithmic accuracy by extending the results presented in Ref. [110] to the case of an additional $k_t^{\min}$ selection. In regards to the heavy-ion scenario, the present Monte Carlo study has informed us about the feasibility to perturbatively describe the high-k_t regime, which motivates carrying out analytic calculations, including medium-induced effects, that can be sensibly confronted with experimental data.

We are confident that an experimental realization of the proposed strategy will provide new key inputs to improve our understanding of the rich interplay between the vacuum and medium scales that govern jet evolution in the quark-gluon plasma.

ACKNOWLEDGMENTS

The authors would like to thank the organizers of the "QCD challenges from pp to AA workshop" which took place in Padova, Italy, where this collaboration started. We also thank Jack Holguin for participating in the early stages of this project and his feedback on the manuscript. We are grateful to Paul Caucal for providing the JetMed samples and comments on the manuscript, Luca Rottoli for providing the Powheg samples, and Silvia Ferrario-Ravasio, Aidin Masouminia, and Simon Plätzer for helping with the HERWIG results. The work of L. C. M. was supported by the European Research Council Project No. ERC-2020-COG-101002207 QCDHighDensityCMS. The work of D. P. has received funding from the European Union's

[11] See footnote 2 for an extended discussion on selection bias effects.

Horizon 2020 research and innovation program under the Marie Sklodowska-Curie Grant Agreement No. 754496. The work of A. S. O. has been funded by the European Research Council (ERC) under the European Union's Horizon 2020 research and innovation program (Grant Agreement No. 788223). The work of M. S. has been supported by the Ministry of Education, Youth and Sports of the Czech Republic under Grant No. ERC-CZ LL2327. The work of A. T. is supported by the Starting Grant from Trond Mohn Foundation (Grant No. BFS2018REK01), the University of Bergen, and by DFG—Project No. 496831614. The work of M. V. was supported by the Dutch Research Council (NWO)—Project No. STU.019.019.

APPENDIX A: EXPERIMENTAL CONSIDERATIONS

Here we address the experimental feasibility of the proposed observable. To start with, this would be the first triple-differential measurement in heavy-ion collisions, i.e., the measurement will require the simultaneous unfolding of background and detector effects in three quantities, p_t^{jet}, k_t^{min}, and θ_{hard}. However, since only thresholds on jet p_t and k_t are imposed, the unfolding problem is simpler than when performing the triple differential measurement over many bins.

An important aspect when correcting the measurement to particle level is the fraction of fake splittings (splittings originating entirely from upward fluctuations of the underlying event). We have estimated the fraction of fake-splittings in our observable by embedding PYTHIA8 events into a thermal background mimicking the underlying event of a heavy-ion collision. The results are shown in the left panel of Fig. 8 after applying full event constituent subtraction [111] to the embedded jets. Jet substructure measurements have been reported for fake fractions smaller than 20%. This threshold is met by our observable as long as $k_t^{\text{min}} \gtrsim 2$ GeV. ALICE studies of the dynamically groomed k_t have shown that for $R = 0.2$ jets in central collisions, a detector-level cutoff of $k_t > 1.5$ GeV renders the observable unfoldable. Due to the strong migrations in k_T between detector and true levels, the fully corrected results can be reported at $p_t = 60$ GeV and $k_t > 3$ GeV in central collisions [112]. The higher jet p_t required in our study implies higher purities and thus we conclude that unfolding this triple-differential observable should not be accompanied by large systematic uncertainties.

Other challenges to realize experimentally the scan of the emission phase space described in the previous sections concern the ability to measure small-angle splittings. Track-based measurements of the Lund plane by ATLAS [114], CMS [115], and ALICE [116] have demonstrated the ability to reconstruct splittings down to angles $\theta \approx 0.005$ and should therefore provide sufficient sensibility to color coherence effects.

In this study, jets were required to have $p_t > 400$ GeV. For LHC runs 3 and 4, assuming total collected luminosity of 13 nb^{-1} [117], we estimated the total number of $R = 0.2$ jets with $p_t > 400$ GeV within $|\eta| < 2.8$ to exceed 1.5×10^4 in 0–10% central PbPb collisions. The estimate is based on the data published in Ref. [43]. The right panel of Fig. 8 shows the expected statistical uncertainty of the θ_{hard} distribution with this projected statistics obtained with Monte Carlo simulations. We would like to remark that reducing the jet p_t selection down to 200 GeV can increase

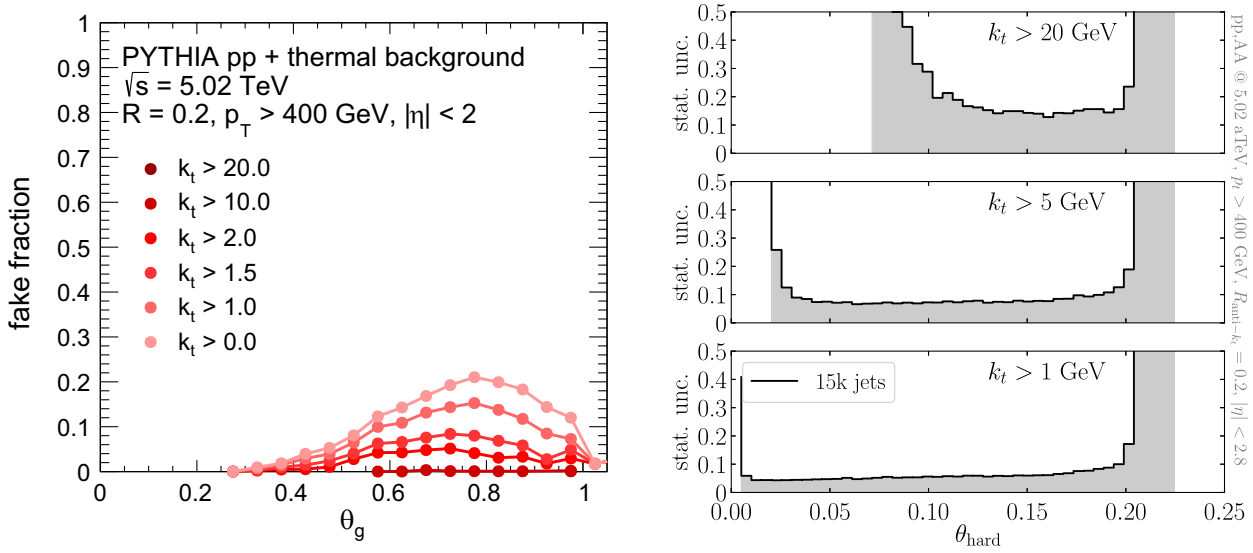

FIG. 8. *Left*: fraction of fake splittings obtained by embedding PYTHIA8 pp events in a thermal background [88,113] for various minimum selections of k_t. *Right*: the relative statistical uncertainty of the θ_{hard} distribution by considering the experimentally accessible number of jets in runs 3 and 4 of the LHC.

the statistics by a factor of 50. The exact jet p_t selection is thus to be decided by experiments based on the available luminosity and effects seen in the data.

APPENDIX B: THE REDUCTION OF BIAS EFFECTS AT HIGH $k_t^{\min}$

The absence of selection bias at high-$k_t^{\min}$ values can be understood based on simple considerations. The object of interest is the energy lost by a jet featuring a splitting with $k_{t,\text{hard}} > k_t^{\min}$ as a function of its opening angle θ_{hard}, which we denote $W(\theta_{\text{hard}}, k_t^{\min})$. The amount of energy lost is directly proportional to the size of the resolved phase space [118], which at $\mathcal{O}(\alpha_s)$ reads

$$\Omega(k_{t,\text{hard}}) = \int_0^R d\theta \int_0^{k_{t,\text{hard}}} dk_t \frac{2C_i\alpha_s(k_t)}{\pi}\frac{d\sigma}{dk_t d\theta} \times \Theta(t_f < L)\Theta(t_f < t_d), \tag{B1}$$

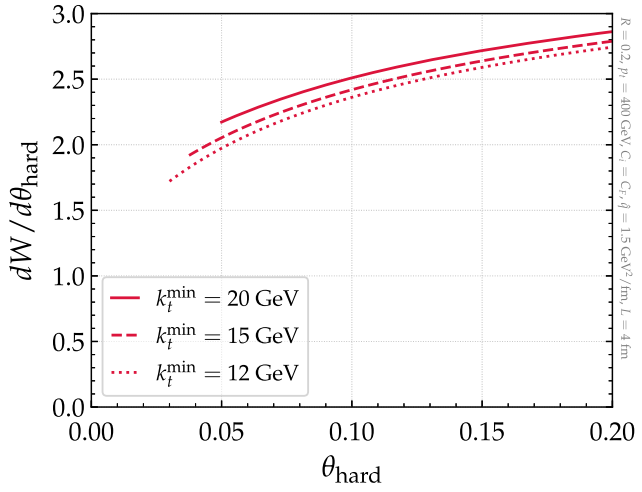

FIG. 9. Size of resolved phase space for jets with $R = 0.2$, $p_t > 400$ GeV as a function of θ_{hard} for different $k_t^{\min}$ values (corresponding to splittings with $\theta > \theta_c$) in the soft-and-collinear limit, see Eq. (B2).

where $d^2\sigma/dk_t d\theta$ is the double-differential cross section for producing a vacuumlike splitting (stripped off color factor and coupling) and the second line of the equation contains all phase-space constraints required for an emission to be part of the resolved phase space. In order to estimate the amount of energy loss differential in angle, this quenched phase space has to be weighted by the cross section for producing the tagged splitting, i.e.,

$$\left.\frac{dW}{d\theta_{\text{hard}}}\right|_{k_t^{\min}} = \frac{\int_{k_t^{\min}}^{p_t\theta_{\text{hard}}} dk_{t,\text{hard}}\,\frac{1}{\sigma}\frac{d\sigma}{dk_{t,\text{hard}}d\theta_{\text{hard}}}\,\Omega(k_{t,\text{hard}})}{\int_{k_t^{\min}}^{p_t\theta_{\text{hard}}} dk_{t,\text{hard}}\,\frac{1}{\sigma}\frac{d\sigma}{dk_{t,\text{hard}}d\theta_{\text{hard}}}}. \tag{B2}$$

In the soft-and-collinear approximation and at fixed-coupling, Eq. (B2) can be solved analytically and the result is plotted in Fig. 9 for a quark jet. We observe that for $k_t^{\min} = 20$ GeV, the size of the quenched phase space is largely independent of θ_{hard} thus confirming the picture drawn by the Monte Carlo generators in Fig. 5. We note that only $k_t^{\min}$ values for which $\theta^{\min} > \theta_c$ are shown in the figure. This is so due to the toy model not being applicable when both resolved and unresolved splittings contribute.

APPENDIX C: L_{res} DEPENDENCE OF HYBRID RESULTS

The HYBRID model allows for smoothly changing the size of the resolved phase space by varying the L_{res} parameter. In Fig. 10 we show the θ_{hard} distribution for all $k_t^{\min}$ values in three different scenarios: only the jet initiator is quenched, $L_{\text{res}} = \infty$ (fully coherent energy loss), all particles are quenched inside the medium, $L_{\text{res}} = 0$ (fully incoherent energy loss), and the intermediate scenario present in the main text in which splittings whose transverse size satisfy $r_{\perp,\text{dip}} > L_{\text{res}} = 2/(\pi T)$ are resolved and lose energy. For the highest value of $k_t^{\min}$ we observe that the resulting θ_{hard} distribution is barely dependent on L_{res} thus confirming that, in this corner of phase space, energy loss details are not relevant and that the ingredient at

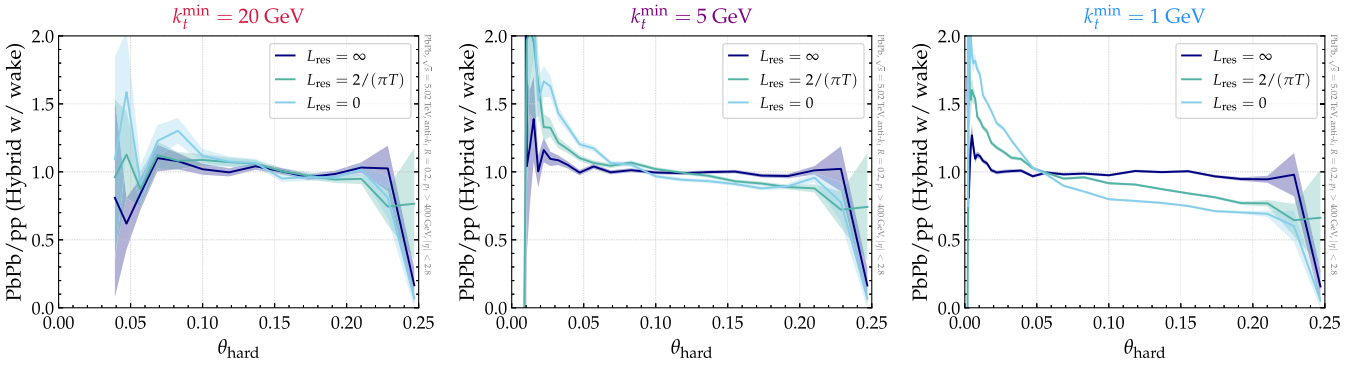

FIG. 10. Sensitivity of HYBRID results to the value of the resolution length L_{res}. From left to right the value of $k_t^{\min}$ decreases.

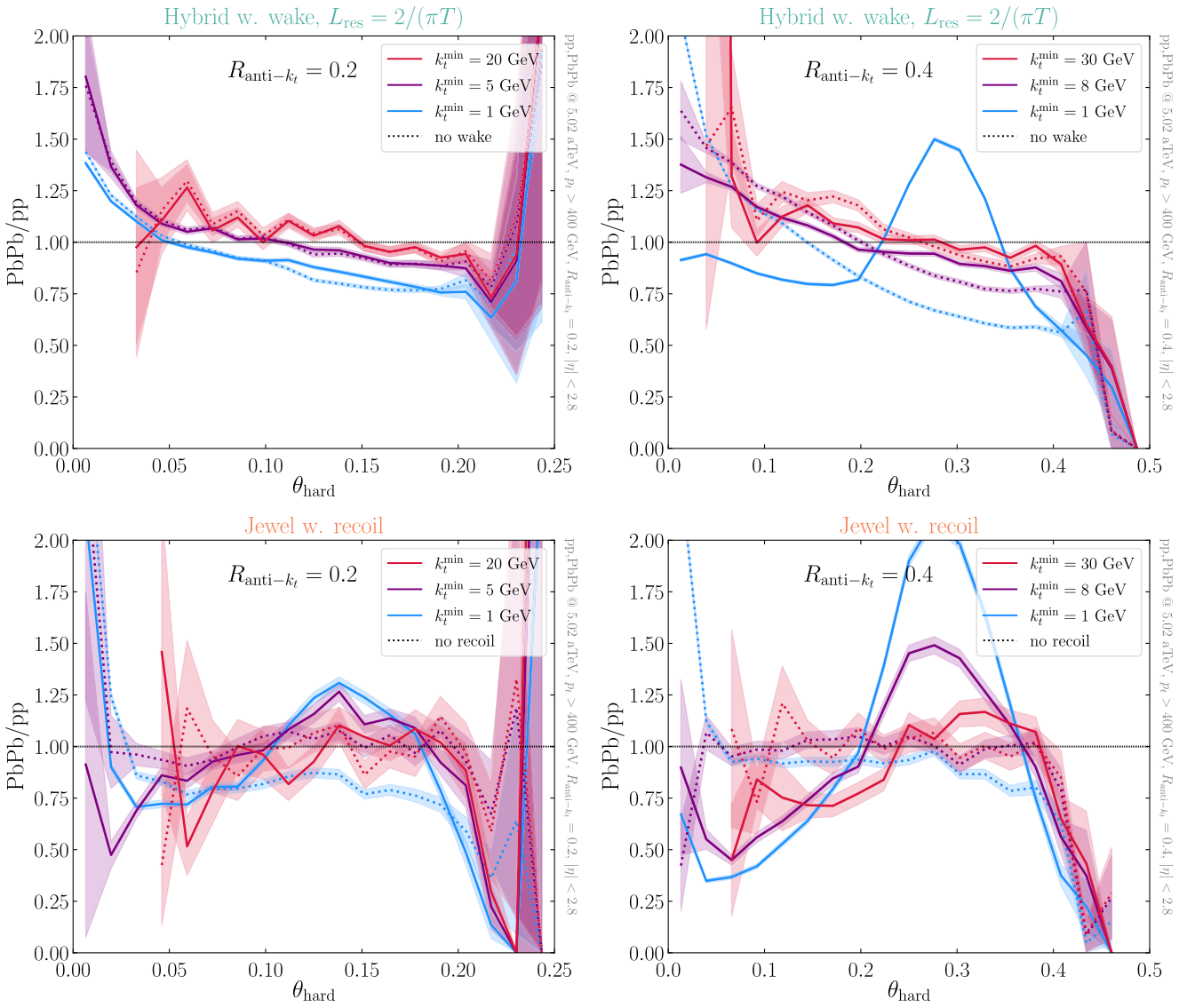

FIG. 11. Same as the ratio plots in Figs. 5, 6, and 7. The upper panels are HYBRID events with and without the wake for different $k_t^{\rm min}$. The lower panels are JEWEL events with and without keeping track of recoilers for different $k_t^{\rm min}$. The left and right side are jets with different cone sizes $R = 0.2$ and $R = 0.4$.

test is the vacuum splitting evolution.[12] By lowering $k_t^{\rm min}$ the observable becomes sensitive to the correlation between energy loss and jet substructure. In fact, $L_{\rm res} = \infty$ yields no in-medium modification as it is independent of the jet substructure. A finite value of $L_{\rm res}$ results in a narrowing of the distribution since more collimated jets tend to lose less energy. This result endorses the potential of the proposed observable to test the presence of an angular scale that controls the degree of quenching, i.e., the medium resolution power. Setting $L_{\rm res} = 0$ (corresponding to all splittings with $t_f < L$ losing energy) leads to an even stronger narrowing of the $\theta_{\rm hard}$ distribution. In this case, the resolution boundary does not fluctuate with temperature and/or parton energy, resulting in a sharper enhancement.

[12]There is still some ordering among different $L_{\rm res}$, which disappears for $R = 0.4$ jets, and thus has its origin in statistical fluctuations occurring for $R = 0.2$.

APPENDIX D: MEDIUM RESPONSE IN JEWEL AND HYBRID

In this section, we study the sensitivity of the proposed observable to medium response effects in the HYBRID and JEWEL models. We remind the reader that JetMed does not account for this effect. In the main text figures we included the HYBRID wake, while discarded JEWEL recoils.

In Fig. 11 we show the PbPb/pp ratio of the $\theta_{\rm hard}$ distributions with and without medium response for both

HYBRID and JEWEL models (similar to the ratio plots in Figs. 5, 6, and 7). The results of the HYBRID model (upper left panel in Fig. 11) suggest that the medium response effects remain below 10% across all $k_t^{\min}$ choices for $R = 0.2$ jets. The reason is that in the HYBRID model all lost energy is assumed to thermalize instantly and contributes as a source term in the hydrodynamic equations of motion. Perturbative, hard elastic scatterings are neglected in the present version of HYBRID, and the resulting medium response is a soft, wide-angle hadron distribution from the wake. To further illustrate wake effects in HYBRID, we repeat the previous plot for wider, $R = 0.4$ jets (upper right panel in Fig. 11). Here, the wake becomes substantially more important at lower $k_t^{\min}$ cuts, implying that the wake appears at wide angles ($\theta > 0.2$). We would like to remind the reader that the overall decreasing trend of the PbPb/pp ratio with increasing angle is caused by the substructure-dependent energy loss and selection bias effects as we discussed in the main text. The effect from medium response sits on top of this effect, typically at larger angles.

JEWEL implements medium response in a radically different manner. The medium response dynamics can affect the θ_{hard} distribution even for moderate $k_t^{\min}$ value (lower left panel in Fig. 11). The size of this effect can reach up to 50% for $k_t^{\min} = 1$ GeV for $R = 0.2$. These recoils are thermal particles that become part of correlated background after undergoing elastic $2 \to 2$ scatterings with the jet particles. These scatterings can be perturbative or not depending on the exchanged momentum.[13] Therefore, the medium response in JEWEL produces harder particles at smaller angles than the wake in HYBRID. Two technical details on the treatment of these recoils are relevant: we have used the method presented in Ref. [121] to ensure energy-momentum conservation (subtracting "holes"). Also, in our runs (default in JEWEL), further rescatterings and splittings of recoil particles are neglected, and they free stream. In the most recent version of JEWEL, recoil rescatterings can be activated. Due to the associated computational cost, we did not consider it here. Recoil in JEWEL therefore implements the other extreme scenario, a completely weakly coupled medium response. To further illustrate the impact of recoil in JEWEL, we repeated the analysis for wider $R = 0.4$ jets. In this case, even the highest $k_t^{\min} = 30$ GeV cut is sensitive to recoil particles, evidencing the stark consequences of the free streaming setup adopted in the present JEWEL study. This is the reason why we did not include the JEWEL recoils in the main text. Indeed, it would be very instructive to test more realistic modeling of medium response, where rescatterings can occur, for instance using kinetic theory [35,122]. Differences in the PbPb/pp ratio between HYBRID and JEWEL in the absence of medium response are due to the different energy loss mechanisms adopted by each model, where in particular one observes a flatter ratio in JEWEL than in HYBRID.

To sum up, our observable not only separates perturbative from nonperturbative effects in terms of radiation and energy loss, but it is also sensitive to the physics of perturbative scatterings and the thermalization process of jets. The choice of using jets with high-enough p_t is in fact crucial, as it allows enough phase space for large-momentum transfer, and thus perturbative, scatterings with the thermal QGP constituents to occur. Measuring this observable in experiments will in this way serve to guide the modeling of medium response in Monte Carlo event generators.

APPENDIX E: CHOICE OF RECLUSTERING ALGORITHM

The observable introduced in this work follows the standard procedure in jet substructure studies by using the anti-k_t algorithm to define jets and then reclustering each jet using the C/A sequence. Phenomenologically, each choice of reclustering algorithm corresponds to a different observable. Some of these choices are easier to handle in analytic computations. For example, the use of C/A is favored from the theoretical point of view since it corresponds to angular ordering, a fundamental property of QCD matrix elements. Depending on the observable, other reclustering algorithms might prove to be more useful from an experimental point of view, but can be more complicated to connect to analytic calculations. Theoretically, the choice of reclustering algorithm enters as a next-double-logarithmic correction as was shown, for example, in Refs. [45,110,123]. We note that this is beyond the current accuracy of jet quenching calculations.

Figure 12 shows the sensitivity of the θ_{hard}-distribution to the reclustering algorithm using JetMed, one of the Monte Carlo generators presented in the main text. The reclustering algorithms are C/A [71,72] (used in the main text), k_t, anti-k_t [69] and τ [77] ($p = 0.5$ in the generalized-k_t algorithm). All four reclustering algorithms yield different curves, as they correspond to different observables. However, all qualitative features that we have extensively discussed in the main text are independent of the clustering choice. More importantly, the medium-to-vacuum panels indicate that the size of medium modifications does not depend on the reclustering algorithm and, therefore, confirms that we are not introducing any bias in the interpretation of our results as due to the choice of the C/A algorithm.

[13] $2 \to 2$ pQCD scatterings are modified in the QGP due to thermal screening effects typically at small momenta [119,120]. We refer to these soft scatterings as nonperturbative as the plasma temperature is relatively low $T_{\text{QGP}} \sim \Lambda_{\text{QCD}}$.

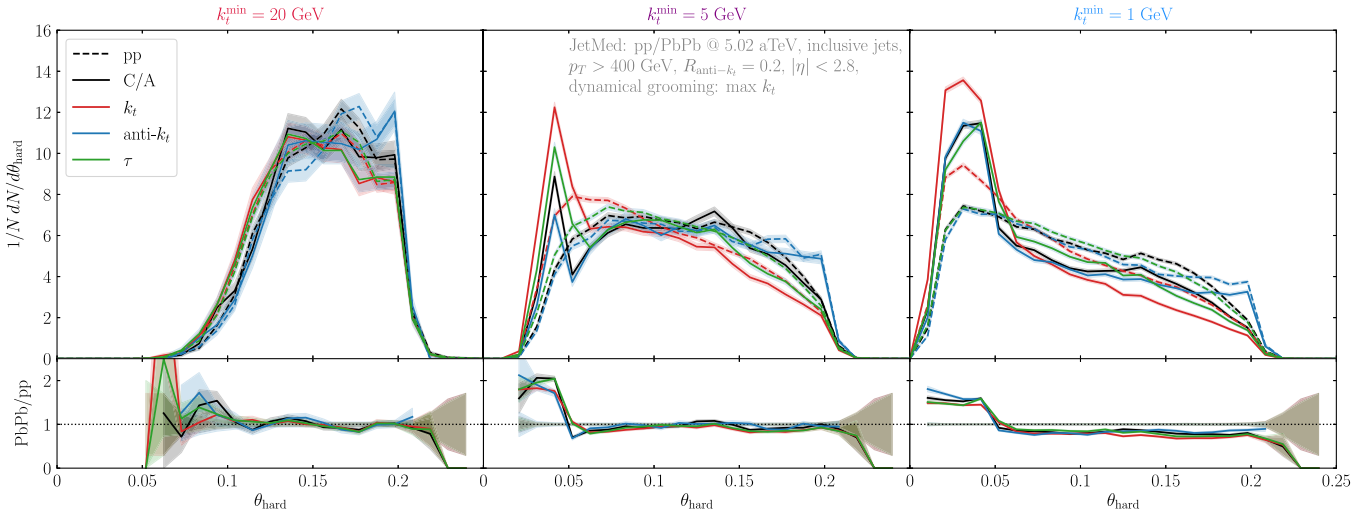

FIG. 12. The impact of different reclustering algorithms on the angular distribution of the hardest splitting inside the jets. Error bands represent only the statistical uncertainty.

[1] N. Armesto and E. Scomparin, Heavy-ion collisions at the Large Hadron Collider: A review of the results from Run 1, Eur. Phys. J. Plus **131**, 52 (2016).

[2] M. Connors, C. Nattrass, R. Reed, and S. Salur, Jet measurements in heavy ion physics, Rev. Mod. Phys. **90**, 025005 (2018).

[3] L. Cunqueiro and A. M. Sickles, Studying the QGP with jets at the LHC and RHIC, Prog. Part. Nucl. Phys. **124**, 103940 (2022).

[4] L. Apolinário, Y.-J. Lee, and M. Winn, Heavy quarks and jets as probes of the QGP, Prog. Part. Nucl. Phys. **127**, 103990 (2022).

[5] ALICE Collaboration, The ALICE experiment—A journey through QCD, arXiv:2211.04384.

[6] J. Casalderrey-Solana and C. A. Salgado, Introductory lectures on jet quenching in heavy ion collisions, Acta Phys. Pol. B **38**, 3731 (2007).

[7] A. Majumder and M. Van Leeuwen, The theory and phenomenology of perturbative QCD based jet quenching, Prog. Part. Nucl. Phys. **66**, 41 (2011).

[8] Y. Mehtar-Tani, J. G. Milhano, and K. Tywoniuk, Jet physics in heavy-ion collisions, Int. J. Mod. Phys. A **28**, 1340013 (2013).

[9] J. J. Ethier and E. R. Nocera, Parton distributions in nucleons and nuclei, Annu. Rev. Nucl. Part. Sci. **70**, 43 (2020).

[10] K. J. Eskola, P. Paakkinen, H. Paukkunen, and C. A. Salgado, EPPS21: A global QCD analysis of nuclear PDFs, Eur. Phys. J. C **82**, 413 (2022).

[11] R. Abdul Khalek, R. Gauld, T. Giani, E. R. Nocera, T. R. Rabemananjara, and J. Rojo, nNNPDF3.0: Evidence for a modified partonic structure in heavy nuclei, Eur. Phys. J. C **82**, 507 (2022).

[12] A. Kurkela and U. A. Wiedemann, Picturing perturbative parton cascades in QCD matter, Phys. Lett. B **740**, 172 (2015).

[13] P. Caucal, E. Iancu, A. H. Mueller, and G. Soyez, Vacuum-like jet fragmentation in a dense QCD medium, Phys. Rev. Lett. **120**, 232001 (2018).

[14] R. Baier, Y. L. Dokshitzer, A. H. Mueller, S. Peigne, and D. Schiff, Radiative energy loss of high-energy quarks and gluons in a finite volume quark—gluon plasma, Nucl. Phys. **B483**, 291 (1997).

[15] B. Zakharov, Fully quantum treatment of the Landau-Pomeranchuk-Migdal effect in QED and QCD, JETP Lett. **63**, 952 (1996).

[16] M. Gyulassy, P. Levai, and I. Vitev, Jet quenching in thin quark gluon plasmas. 1. Formalism, Nucl. Phys. **B571**, 197 (2000).

[17] U. A. Wiedemann, Gluon radiation off hard quarks in a nuclear environment: Opacity expansion, Nucl. Phys. **B588**, 303 (2000).

[18] J. Ghiglieri and D. Teaney, Parton energy loss and momentum broadening at NLO in high temperature QCD plasmas, Int. J. Mod. Phys. E **24**, 1530013 (2015).

[19] S. Schlichting and D. Teaney, The first fm/c of heavy-ion collisions, Annu. Rev. Nucl. Part. Sci. **69**, 447 (2019).

[20] J. Berges, M. P. Heller, A. Mazeliauskas, and R. Venugopalan, QCD thermalization: *Ab initio* approaches and interdisciplinary connections, Rev. Mod. Phys. **93**, 035003 (2021).

[21] B. Andersson, G. Gustafson, G. Ingelman, and T. Sjostrand, Parton fragmentation and string dynamics, Phys. Rep. **97**, 31 (1983).

[22] B. R. Webber, A QCD model for jet fragmentation including soft gluon interference, Nucl. Phys. **B238**, 492 (1984).

[23] A. Beraudo, J. G. Milhano, and U. A. Wiedemann, Medium-induced color flow softens hadronization, Phys. Rev. C **85**, 031901 (2012).

[24] P. M. Chesler, K. Jensen, A. Karch, and L. G. Yaffe, Light quark energy loss in strongly-coupled $N = 4$ supersymmetric Yang-Mills plasma, Phys. Rev. D **79**, 125015 (2009).

[25] S. S. Gubser, D. R. Gulotta, S. S. Pufu, and F. D. Rocha, Gluon energy loss in the gauge-string duality, J. High Energy Phys. 10 (2008) 052.

[26] Y. Hatta, E. Iancu, and A. H. Mueller, Jet evolution in the $N = 4$ SYM plasma at strong coupling, J. High Energy Phys. 05 (2008) 037.

[27] P. Arnold and D. Vaman, Jet quenching in hot strongly coupled gauge theories revisited: 3-point correlators with gauge-gravity duality, J. High Energy Phys. 10 (2010) 099.

[28] P. M. Chesler and K. Rajagopal, Jet quenching in strongly coupled plasma, Phys. Rev. D **90**, 025033 (2014).

[29] I. P. Lokhtin and A. M. Snigirev, A model of jet quenching in ultrarelativistic heavy ion collisions and high-p(T) hadron spectra at RHIC, Eur. Phys. J. C **45**, 211 (2006).

[30] K. Zapp, G. Ingelman, J. Rathsman, J. Stachel, and U. A. Wiedemann, A Monte Carlo model for 'Jet Quenching', Eur. Phys. J. C **60**, 617 (2009).

[31] N. Armesto, L. Cunqueiro, and C. A. Salgado, Q-PYTHIA: A medium-modified implementation of final state radiation, Eur. Phys. J. C **63**, 679 (2009).

[32] J. Casalderrey-Solana, J. G. Milhano, and P. Quiroga-Arias, Out of medium fragmentation from long-lived jet showers, Phys. Lett. B **710**, 175 (2012).

[33] B. Schenke, C. Gale, and S. Jeon, MARTINI: An event generator for relativistic heavy-ion collisions, Phys. Rev. C **80**, 054913 (2009).

[34] A. Majumder, Incorporating space-time within medium-modified jet event generators, Phys. Rev. C **88**, 014909 (2013).

[35] X.-N. Wang and Y. Zhu, Medium modification of γ-jets in high-energy heavy-ion collisions, Phys. Rev. Lett. **111**, 062301 (2013).

[36] J. Casalderrey-Solana, D. C. Gulhan, J. G. Milhano, D. Pablos, and K. Rajagopal, A HYBRID strong/weak coupling approach to jet quenching, J. High Energy Phys. 10 (2015) 019; 09 (2015) 175(E).

[37] C. Bierlich, G. Gustafson, L. Lönnblad, and H. Shah, The angantyr model for heavy-ion collisions in PYTHIA8, J. High Energy Phys. 10 (2018) 134.

[38] W. Ke and X.-N. Wang, QGP modification to single inclusive jets in a calibrated transport model, J. High Energy Phys. 05 (2021) 041.

[39] Y. Tachibana *et al.* (JETSCAPE Collaboration), Hard jet substructure in a multi-stage approach, arXiv:2301.02485.

[40] N. Armesto, G. Corcella, L. Cunqueiro, and C. A. Salgado, Angular-ordered parton showers with medium-modified splitting functions, J. High Energy Phys. 11 (2009) 122.

[41] K. C. Zapp, F. Krauss, and U. A. Wiedemann, A perturbative framework for jet quenching, J. High Energy Phys. 03 (2013) 080.

[42] S. Acharya *et al.* (A Large Ion Collider Experiment and ALICE Collaborations), Measurement of the groomed jet radius and momentum splitting fraction in pp and Pb-Pb collisions at $\sqrt{s_{NN}} = 5.02$ TeV, Phys. Rev. Lett. **128**, 102001 (2022).

[43] ATLAS Collaboration, Measurement of suppression of large-radius jets and its dependence on substructure in Pb + Pb collisions at $\sqrt{s_{\mathrm{NN}}} = 5.02$ TeV with the ATLAS detector, Phys. Rev. Lett. **131**, 172301 (2023).

[44] A. Hayrapetyan, Girth and groomed radius of jets recoiling against isolated photons in lead-lead and proton-proton collisions at $\sqrt{s_{\mathrm{NN}}} = 5.02$TeV, arXiv:2405.02737.

[45] F. A. Dreyer, G. P. Salam, and G. Soyez, The Lund jet plane, J. High Energy Phys. 12 (2018) 064.

[46] Y. L. Dokshitzer, V. A. Khoze, A. H. Mueller, and S. I. Troian, *Basics of Perturbative QCD* (Editions Frontieres, Gif-sur-Yvette, 1991).

[47] G. Altarelli and G. Parisi, Asymptotic freedom in parton language, Nucl. Phys. **B126**, 298 (1977).

[48] X.-N. Wang, M. Gyulassy, and M. Plumer, The LPM effect in QCD and radiative energy loss in a quark gluon plasma, Phys. Rev. D **51**, 3436 (1995).

[49] C. Andrés, N. Armesto, M. Luzum, C. A. Salgado, and P. Zurita, Energy versus centrality dependence of the jet quenching parameter $\hat{q}$ at RHIC and LHC: A new puzzle?, Eur. Phys. J. C **76**, 475 (2016).

[50] X. Feal, C. A. Salgado, and R. A. Vazquez, Jet quenching test of the QCD matter created at RHIC and the LHC needs opacity-resummed medium induced radiation, Phys. Lett. B **816**, 136251 (2021).

[51] S. Cao *et al.* (JETSCAPE Collaboration), Determining the jet transport coefficient $\hat{q}$ from inclusive hadron suppression measurements using Bayesian parameter estimation, Phys. Rev. C **104**, 024905 (2021).

[52] X.-N. Wang and X.-f. Guo, Multiple parton scattering in nuclei: Parton energy loss, Nucl. Phys. **A696**, 788 (2001).

[53] F. D'Eramo, K. Rajagopal, and Y. Yin, Molière scattering in quark-gluon plasma: Finding point-like scatterers in a liquid, J. High Energy Phys. 01 (2019) 172.

[54] Y. Mehtar-Tani, C. A. Salgado, and K. Tywoniuk, Anti-angular ordering of gluon radiation in QCD media, Phys. Rev. Lett. **106**, 122002 (2011).

[55] J. Casalderrey-Solana and E. Iancu, Interference effects in medium-induced gluon radiation, J. High Energy Phys. 08 (2011) 015.

[56] K. Rajagopal, A. V. Sadofyev, and W. van der Schee, Evolution of the jet opening angle distribution in holographic plasma, Phys. Rev. Lett. **116**, 211603 (2016).

[57] J. Brewer, J. G. Milhano, and J. Thaler, Sorting out quenched jets, Phys. Rev. Lett. **122**, 222301 (2019).

[58] J. Brewer, J. Thaler, and A. P. Turner, Data-driven quark and gluon jet modification in heavy-ion collisions, Phys. Rev. C **103**, L021901 (2021).

[59] J. Brewer, Q. Brodsky, and K. Rajagopal, Disentangling jet modification in jet simulations and in Z + jet data, J. High Energy Phys. 02 (2022) 175.

[60] A. Takacs and K. Tywoniuk, Quenching effects in the cumulative jet spectrum, J. High Energy Phys. 10 (2021) 038.

[61] D. Pablos and A. Soto-Ontoso, Pushing forward jet substructure measurements in heavy-ion collisions, Phys. Rev. D **107**, 094003 (2023).

[62] M. Spousta and B. Cole, Interpreting single jet measurements in Pb + Pb collisions at the LHC, Eur. Phys. J. C **76**, 50 (2016).

[63] J.-W. Qiu, F. Ringer, N. Sato, and P. Zurita, Factorization of jet cross sections in heavy-ion collisions, Phys. Rev. Lett. **122**, 252301 (2019).

[64] F. Ringer, B.-W. Xiao, and F. Yuan, Can we observe jet P_T-broadening in heavy-ion collisions at the LHC?, Phys. Lett. B **808**, 135634 (2020).

[65] P. Caucal, A. Soto-Ontoso, and A. Takacs, Dynamically groomed jet radius in heavy-ion collisions, Phys. Rev. D **105**, 114046 (2022).

[66] G. Aad *et al.* (ATLAS Collaboration), Measurement of substructure-dependent jet suppression in Pb + Pb collisions at 5.02 TeV with the ATLAS detector, Phys. Rev. C **107**, 054909 (2023).

[67] T. Liou, A. H. Mueller, and B. Wu, Radiative $p_\perp$-broadening of high-energy quarks and gluons in QCD matter, Nucl. Phys. **A916**, 102 (2013).

[68] J.-P. Blaizot and Y. Mehtar-Tani, Renormalization of the jet-quenching parameter, Nucl. Phys. **A929**, 202 (2014).

[69] M. Cacciari, G. P. Salam, and G. Soyez, The anti-k_t jet clustering algorithm, J. High Energy Phys. 04 (2008) 063.

[70] M. Cacciari, G. P. Salam, and G. Soyez, FastJet user manual, Eur. Phys. J. C **72**, 1896 (2012).

[71] Y. L. Dokshitzer, G. D. Leder, S. Moretti, and B. R. Webber, Better jet clustering algorithms, J. High Energy Phys. 08 (1997) 001.

[72] M. Wobisch and T. Wengler, Hadronization corrections to jet cross-sections in deep inelastic scattering, in *Proceedings of the Workshop on Monte Carlo Generators for HERA Physics* (1998), pp. 270–279, arXiv:hep-ph/9907280.

[73] J. Casalderrey-Solana, Y. Mehtar-Tani, C. A. Salgado, and K. Tywoniuk, New picture of jet quenching dictated by color coherence, Phys. Lett. B **725**, 357 (2013).

[74] Y. Mehtar-Tani, A. Soto-Ontoso, and K. Tywoniuk, Dynamical grooming of QCD jets, Phys. Rev. D **101**, 034004 (2020).

[75] L. Wang, J.-W. Kang, Q. Zhang, S. Shen, W. Dai, B.-W. Zhang, and E. Wang, Jet radius and momentum splitting fraction with dynamical grooming in heavy-ion collisions, Chin. Phys. Lett. **40**, 032101 (2023).

[76] S. Acharya *et al.* (ALICE Collaboration), Measurements of the groomed jet radius and momentum splitting fraction with the soft drop and dynamical grooming algorithms in pp collisions at $\sqrt{s} = 5.02$ TeV, J. High Energy Phys. 05 (2023) 244.

[77] L. Apolinário, A. Cordeiro, and K. Zapp, Time reclustering for jet quenching studies, Eur. Phys. J. C **81**, 561 (2021).

[78] L. Apolinário, R. Kunnawalkam Elayavalli, and N. Olavo, Transitioning from perturbative to non-perturbative splittings within QCD jets, arXiv:2212.11846.

[79] L. Cunqueiro, D. Napoletano, and A. Soto-Ontoso, Dead-cone searches in heavy-ion collisions using the jet tree, Phys. Rev. D **107**, 094008 (2023).

[80] A. J. Larkoski, S. Marzani, G. Soyez, and J. Thaler, Soft Drop, J. High Energy Phys. 05 (2014) 146.

[81] Y. Mehtar-Tani and K. Tywoniuk, Groomed jets in heavy-ion collisions: Sensitivity to medium-induced bremsstrahlung, J. High Energy Phys. 04 (2017) 125.

[82] Y.-T. Chien and I. Vitev, Probing the hardest branching within jets in heavy-ion collisions, Phys. Rev. Lett. **119**, 112301 (2017).

[83] G. Milhano, U. A. Wiedemann, and K. C. Zapp, Sensitivity of jet substructure to jet-induced medium response, Phys. Lett. B **779**, 409 (2018).

[84] J. Casalderrey-Solana, G. Milhano, D. Pablos, and K. Rajagopal, Modification of jet substructure in heavy ion collisions as a probe of the resolution length of quark-gluon plasma, J. High Energy Phys. 01 (2020) 044.

[85] A. M. Sirunyan *et al.* (CMS Collaboration), Measurement of the splitting function in pp and Pb-Pb collisions at $\sqrt{s_{\mathrm{NN}}} = 5.02$ TeV, Phys. Rev. Lett. **120**, 142302 (2018).

[86] J. Adam *et al.* (STAR Collaboration), Measurement of groomed jet substructure observables in p + p collisions at $\sqrt{s} = 200$ GeV with STAR, Phys. Lett. B **811**, 135846 (2020).

[87] A. M. Sirunyan *et al.* (CMS Collaboration), Measurement of the groomed jet mass in PbPb and pp collisions at $\sqrt{s_{\mathrm{NN}}} = 5.02$ TeV, J. High Energy Phys. 10 (2018) 161.

[88] H. A. Andrews *et al.*, Novel tools and observables for jet physics in heavy-ion collisions, J. Phys. G **47**, 065102 (2020).

[89] C. Andres, F. Dominguez, R. Kunnawalkam Elayavalli, J. Holguin, C. Marquet, and I. Moult, Resolving the scales of the quark-gluon plasma with energy correlators, Phys. Rev. Lett. **130**, 262301 (2023).

[90] C. Andres, F. Dominguez, J. Holguin, C. Marquet, and I. Moult, A coherent view of the quark-gluon plasma from energy correlators, J. High Energy Phys. 09 (2023) 088.

[91] S. Alioli, K. Hamilton, P. Nason, C. Oleari, and E. Re, Jet pair production in POWHEG, J. High Energy Phys. 04 (2011) 081.

[92] C. Bierlich *et al.*, A comprehensive guide to the physics and usage of PYTHIA8.3, SciPost Phys. Codebases **2022**, 8 (2022).

[93] J. Alwall, R. Frederix, S. Frixione, V. Hirschi, F. Maltoni, O. Mattelaer, H. S. Shao, T. Stelzer, P. Torrielli, and M. Zaro, The automated computation of tree-level and next-to-leading order differential cross sections, and their matching to parton shower simulations, J. High Energy Phys. 07 (2014) 079.

[94] J. Bellm *et al.*, HERWIG7.0/HERWIG++ 3.0 release note, Eur. Phys. J. C **76**, 196 (2016).

[95] P. Caucal, E. Iancu, and G. Soyez, Deciphering the z_g distribution in ultrarelativistic heavy ion collisions, J. High Energy Phys. 10 (2019) 273.

[96] T. Sjostrand, S. Mrenna, and P. Z. Skands, PYTHIA6.4 physics and manual, J. High Energy Phys. 05 (2006) 026.

[97] P. Caucal, E. Iancu, and G. Soyez, Jet radiation in a longitudinally expanding medium, J. High Energy Phys. 04 (2021) 209.

[98] J. Casalderrey-Solana, D. C. Gulhan, J. G. Milhano, D. Pablos, and K. Rajagopal, Predictions for boson-jet observables and fragmentation function ratios from a HYBRID strong/weak coupling model for jet quenching, J. High Energy Phys. 03 (2016) 053.
[99] P. M. Chesler and K. Rajagopal, On the evolution of jet energy and opening angle in strongly coupled plasma, J. High Energy Phys. 05 (2016) 098.
[100] C. Shen, Z. Qiu, H. Song, J. Bernhard, S. Bass, and U. Heinz, The iEBE-VISHNU code package for relativistic heavy-ion collisions, Comput. Phys. Commun. **199**, 61 (2016).
[101] M. L. Miller, K. Reygers, S. J. Sanders, and P. Steinberg, Glauber modeling in high energy nuclear collisions, Annu. Rev. Nucl. Part. Sci. **57**, 205 (2007).
[102] Z. Hulcher, D. Pablos, and K. Rajagopal, Resolution effects in the HYBRID strong/weak coupling model, J. High Energy Phys. 03 (2018) 010.
[103] J. Casalderrey-Solana, D. Gulhan, G. Milhano, D. Pablos, and K. Rajagopal, Angular structure of jet quenching within a HYBRID strong/weak coupling model, J. High Energy Phys. 03 (2017) 135.
[104] G. Ovanesyan and I. Vitev, An effective theory for jet propagation in dense QCD matter: Jet broadening and medium-induced bremsstrahlung, J. High Energy Phys. 06 (2011) 080.
[105] A. Kumar *et al.* (JETSCAPE Collaboration), Inclusive jet and hadron suppression in a multistage approach, Phys. Rev. C **107**, 034911 (2023).
[106] Y.-L. Du, D. Pablos, and K. Tywoniuk, Deep learning jet modifications in heavy-ion collisions, J. High Energy Phys. 03 (2021) 206.
[107] Y. Mehtar-Tani, D. Pablos, and K. Tywoniuk, Cone-size dependence of jet suppression in heavy-ion collisions, Phys. Rev. Lett. **127**, 252301 (2021).
[108] N. Armesto, C. A. Salgado, and U. A. Wiedemann, Medium induced gluon radiation off massive quarks fills the dead cone, Phys. Rev. D **69**, 114003 (2004).
[109] C. Andres, F. Dominguez, J. Holguin, C. Marquet, and I. Moult, Seeing beauty in the quark-gluon plasma with energy correlators, arXiv:2307.15110.
[110] P. Caucal, A. Soto-Ontoso, and A. Takacs, Dynamical grooming meets LHC data, J. High Energy Phys. 07 (2021) 020.
[111] P. Berta, M. Spousta, D. W. Miller, and R. Leitner, Particle-level pileup subtraction for jets and jet shapes, J. High Energy Phys. 06 (2014) 092.
[112] R. Ehlers (ALICE Collaboration), Exploring medium properties with hard transverse momentum splittings using groomed jet substructure measurements in Pb–Pb collisions with ALICE, *Proc. Sci.*, HardProbes2023 (2024) 136 [arXiv:2310.07065].
[113] J. Mulligan and M. Ploskon, Identifying groomed jet splittings in heavy-ion collisions, Phys. Rev. C **102**, 044913 (2020).
[114] ATLAS Collaboration (ATLAS Collaboration), Measurement of the Lund jet plane using charged particles in 13 TeV proton-proton collisions with the ATLAS detector, Phys. Rev. Lett. **124**, 222002 (2020).
[115] CMS Collaboration, Measurement of the primary Lund jet plane density in proton-proton collisions at $\sqrt{s} = 13$ TeV, J. High Energy Phys. 05 (2024) 116.
[116] ALICE Collaboration, Physics Preliminary Summary: Measurement of the primary Lund plane density in pp collisions at $\sqrt{s} = 13$ TeV with ALICE (2021).
[117] CERN, *LHC Chamonix Workshop 2023* (2023).
[118] Y. Mehtar-Tani and K. Tywoniuk, Sudakov suppression of jets in QCD media, Phys. Rev. D **98**, 051501 (2018).
[119] J.-P. Blaizot and E. Iancu, The Quark gluon plasma: Collective dynamics and hard thermal loops, Phys. Rep. **359**, 355 (2002).
[120] J. I. Kapusta and C. Gale, *Finite-Temperature Field Theory*, 2nd ed., Cambridge Monographs on Mathematical Physics (Cambridge University Press, Cambridge, England, 2006), 10.1017/CBO9780511535130.
[121] J. G. Milhano and K. Zapp, Improved background subtraction and a fresh look at jet sub-structure in JEWEL, Eur. Phys. J. C **82**, 1010 (2022).
[122] Y. Mehtar-Tani, S. Schlichting, and I. Soudi, Jet thermalization in QCD kinetic theory, J. High Energy Phys. 05 (2023) 091.
[123] A. Lifson, G. P. Salam, and G. Soyez, Calculating the primary Lund jet plane density, J. High Energy Phys. 10 (2020) 170.